AC and DC magnetic properties of zirconium dioxide coated iron oxide nanoparticles

By

Muhammad Shoaib Khan
(312-FBAS/MSPHY/F14)

Supervisor:

Dr. Kashif Nadeem

Assistant Professor

Department of Physics, FBAS, IIUI

Department of Physics Faculty of Basic and Applied Sciences International Islamic University, Islamabad

(2016)

Nanotechnology.

Nanomaterials.

X-ray diffraction.

Magnetic properties.

AC and DC magnetic properties of zirconium dioxide coated iron oxide nanoparticles

By

Muhammad Shoaib Khan

(312-FBAS/MSPHY/F14)

This thesis is submitted to Department of Physics International Islamic University, Islamabad for the award of degree of MS Physics.

CHAIRMAN
DEPT. OF PHYSICS
International Islamic University
Islamabad

2-11-2016.

_____
Chairman Department of Physics   International Islamic University Islamabad

_____
Dean Faculty of Basic and Applied Science International Islamic University,

Islamabad

Final Approval

It is certified that the work printed in this thesis entitled "**AC and DC magnetic properties of zirconium dioxide coated iron Oxide nanoparticles**" by **Muhammad Shoaib Khan**, registration No.312-FBAS/ MSPHY/ F14 is of sufficient standard in scope and quality for award of degree of MS Physics from Department of Physics, International Islamic University, Islamabad, Pakistan.
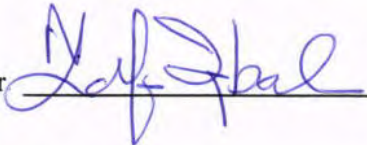
Viva Voce Committee

Chairman (Physics) _____

CHAIRMAN
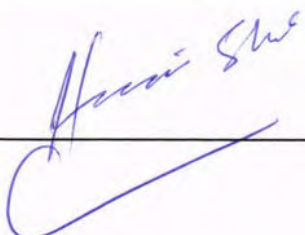DEPT. OF PHYSICS
International Islamic University
Islamabad

Supervisor _____

External Examiner _____

Internal Examiner _____

iii

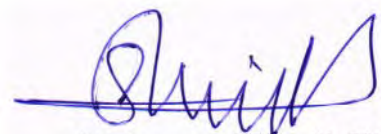بسم الله الرحمن الرحيم

DEDICATED

to

My beloved

Parents and

My

Friends

Declaration

I, **Muhammad Shoaib Khan** (Registration No. 312-FBAS/MSPHY/F14), student of Ms Physics (session 2014-2016), hereby declare that the work presented in the thesis entitled **"AC and DC magnetic properties of zirconium dioxide coated iron oxide nanoparticles"** in partial fulfillment of MS degree in Physics from International Islamic University Islamabad, is my own work and has not been published or submitted as research work or thesis in any form in any other university or institute in Pakistan or abroad.

Muhammad Shoaib Khan

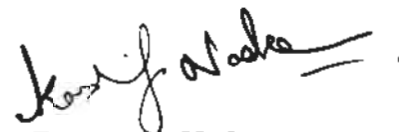(312-FBAS/MSPHY/F14)

Dated: 01-11-2016

FORWARDING SHEET BY RESEARCH SUPERVISOR

The thesis entitled "AC and DC magnetic properties of zirconium dioxide coated iron oxide nanoparticles" submitted by **Muhammad Shoaib Khan** in partial fulfillment of M.S. degree in Physics has been completed under my guidance and supervision. I am satisfied with the quality of student's research work and allow him to submit this thesis for further process to graduate with Master of Science degree from Department of Physics, as per IIU rules and regulations.

Dated: 01 – 11 – 2016

Dr. Kashif Nadeem,
Assistant Professor (TTS)
Department of Physics,
International Islamic
University,
Islamabad.

Acknowledgment

Praise is to **Allah Almighty** who gave me strength and inspiration to complete this research project. Though only my name appears on the cover of this dissertation, but many great people have contributed to its production. I would like to acknowledge the worth mentioning supervision of **Dr. Kashif Nadeem** who guided me and supported me during my whole research work. I am also thankful to **Faisal Zeb** who encouraged me and guided me in productive manner during my research work. Moreover, their supervision enabled me to develop an understanding about the field and without their sincere efforts; I would not be able to complete this hard task of my life. I am again really thankful to **Dr. Kashif Nadeem** for his inspiration and encouragement.

Moreover, I would like to express my sincere thanks to all the faculty members of Department of Physics IIU Islamabad especially to **Dr. Waqar Adil Syed** (Chairman). I would also like to thank all other faculty members of my university for their sincere appreciation, comments and suggestions. I express my thanks to all the staff members of Physics Department, IIU, for their various special services. I shall express my heartiest thanks to all my senior research colleagues **Tariq Jan, Irfan Khan and Adnan Razaq Qureshi** for being very supportive and co-operative throughout my research work. I also pay special thanks to my class fellows **Asmat Ullah, Fahad Ali Shah, Salaudin Kundi, Sajid Khan, Sufaid Shah, Aqeel Khan and Yasir Mehmood**, without their guidance, it was not possible to complete this work.

I wish to express my deep sense of gratitude to my best and beloved friends and all other friends and well wishers for their inspirable guidance and continuous encouragement.

I especially want to acknowledge efforts and prayers of my mother, father, grandmother and aunts for their love, care and support in my life, which has been directly encouraging me for my study. My parents' prayers are always a source of success for me. Allah may bless my parents and family with long life, health and happiness.

Finally, I feel that this acknowledgement is incomplete without paying my cordial gratitude to my beloved friend and cousin **Kifayat Ullah.**

Muhammad Shoaib Khan

Table of Contents

x

List of Figures

List of Tables

ABSTRACT

AC and DC magnetic properties of zirconia (ZrO_2) coated maghemite nanoparticles have been studied by using SQUID magnetic measurements. X-ray diffraction (XRD) analysis showed inverse spinel structure for ZrO_2 coated maghemite nanoparticles. Average crystallite size was calculated to be 14 and 5 nm for maghemite and ZrO_2, respectively. Zero field cooled/field cooled (ZFC/FC) magnetic measurements showed the superparamagnetic blocking temperature (T_B) at 65 K. The coercivity showed an enhanced behavior at 5K which is due to enhanced surface anisotropy at low temperatures. The M-H hysteresis partial loops were not saturated even at 5 T which is also due to enhanced surface spins disorder in these nanoparticles. The increase in saturation magnetization (M_s) with decreasing temperature was fitted by using Bloch's law. Frequency dependent AC susceptibility data showed the decrease in T_B with decreasing AC signal frequency. The shift of T_B with frequency was first analyzed by using thermally activated Arrhenius law. Fitting of Arrhenius law provides non-reasonable values of the atomic spin flip time and thermal activation energy. The same data was analyzed by using Vogel-Fulcher law which gives reasonable value of spin-flip time and interparticle interaction parameter T_0 = 36 K which confirms the moderate interparticle interactions among the nanoparticles. Dynamic scaling law exhibits the suitable fitting to AC susceptibility data, as the dynamic critical exponent (zv) =5.75 takes value between 4 and 12, which is the characteristic of the spin glass system. In summary, all measurements exhibit the significance of enhanced surface effects in ZrO_2 coated maghemite nanoparticles produced by random frozen surface spins.

CHAPTER 1

Introduction

1.1 Nanoscience

Nanoscience is one of the revolutionary field of science where objects and particles at very minute scale are being studied; usually this scale ranges from 1nm to 100nm. Nanoscience is one of the growing research field and advancement to the modern technology. When the matter is divided into very fine particles (at the nanoscale) then its physical properties like electric and magnetic properties are tremendously changes which are usually due to change in size of particles and quantum size effects [1].

1.2 Nanotechnology

Nanotechnology consists of development, structural assembling, fabrication and manipulating of the matter at the nanoscale. Nanotechnology connects all major sciences like physics, biology and chemistry etc. Nanotechnology uses unique physical, mechanical, electrical and chemical properties when matter is fabricated at the nanoscale.
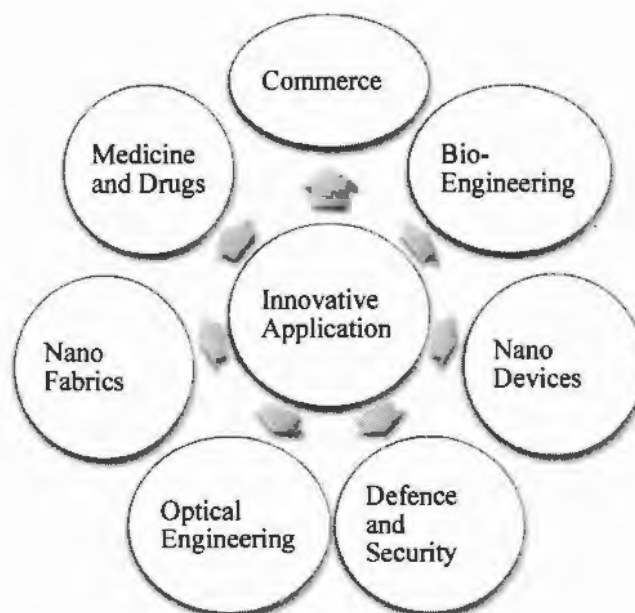
Fig. 1.1: Applications of nanotechnology.

1

Nanotechnology has wide applications in the semiconductor industry, medicines, electronics, biotechnology, tissue engineering, optical engineering, commerce, defense and security which are shown in Fig. 1.1 [2].

1.2.1 History of Nanotechnology

The word "Nano" has been derived from the Greek word "Nanos" which means "Extremely small". The basic idea of nanotechnology is emerged in 1959 when Professor Richard Feynman told that "there is plenty of room at Bottom" in the conference of the American Physical Society at California institute of technology. These small tiny particles are termed as "Mechanical Surgeon" because these have the ability to diagnose and to do the precise surgery of damaged cells by inserting them into the body. Feynman said that we could synthesize things atom by atom using the different laws and rules of physics and chemistry [3].

1.2.2 Nanoparticles

Those particles whose size lies in the range of 1nm to 100 nm in at least one dimensions are said to be nanoparticles. It has the simplest structural size among smaller particles. Nanoparticle is the cluster of atoms bonded together with radius less than 100 nm. High surface energy, high surface to volume size ratio and quantum size effects are some significant properties of the nanoparticles which differentiates their magnetic, optical, electrical and mechanical properties from other bulk particles. Due to high surface energies, nanoparticles have reduced melting points, enhanced mechanical strength and change in optical properties [4].

1.2.3 Nanomaterial

Nanomaterial is the collection of nanoparticles with sizes less than 100 nanometer in at least one dimension. Nanomaterials have significant changes in physical and chemical properties at nanoscale, which is attributed to high surface energy. Fig. 1.2 shows different types of nanostructured materials like nano rods and thin films etc. Magnetic memory effects of nanomaterials are directly dependent upon their sizes. There is great change in surface to volume area ratio as size of the nanomaterial become less than 50 nm [5]. The performance of different materials can be increased if structure and synthesis of nanoparticles are controlled at the nanoscale.

2

Nanostructured materials have wide applications in electronic industry, solar energy industry, optical devices, bio medical devices and fuel cells [6].

Clusters	Nanotubes, fibers and rods	Films and coats	Polycrystals
0D	1D	2D	3D
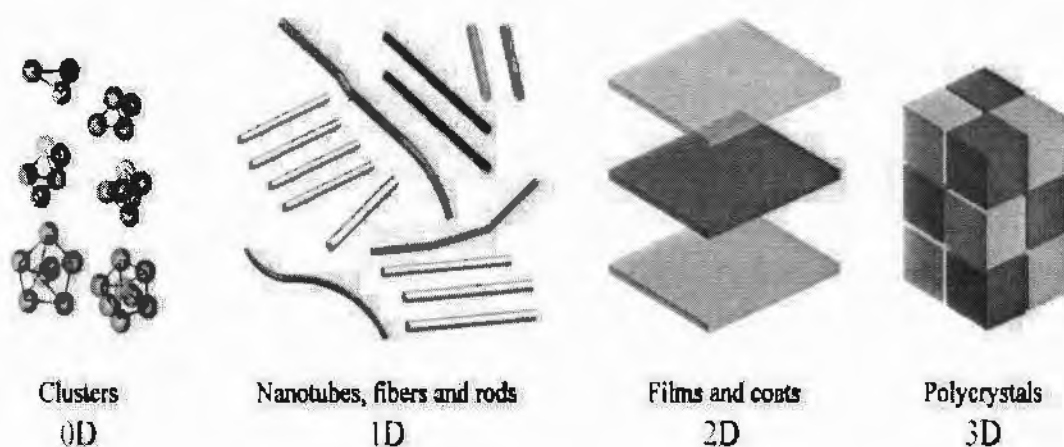
Fig. 1.2: Nanomaterials with different dimensional structures [5].

1.3   Magnetic Nanoparticles

Nanoparticles made from magnetic materials are known as magnetic nanoparticles. Scientists show keen interest in magnetic nanoparticles due to their property of biocompatibility, high saturation magnetization and magnetic susceptibility. Magnetic nanoparticles with surface stabilization are termed as Ferrofluids, which are superparamagnetic in nature having single domain [7].

Fig. 1.3 shows wide applications of magnetic nanoparticles in the field of biotechnology. The change in surface energy by use of surfactant has significant biological effects in fields like bio-sensing, therapeutic analysis, molecular imaging and targeted drug transfer. The medical use of magnetic nanoparticles is a very attractive field for researchers and scientists especially in field of magnetic hyperthermia.

Magnetic nanoparticles for biomedical applications consists the following three parts.

- Magnetic core
- Surface coating
- Bimolecular entity (Anti-disease drug)

3
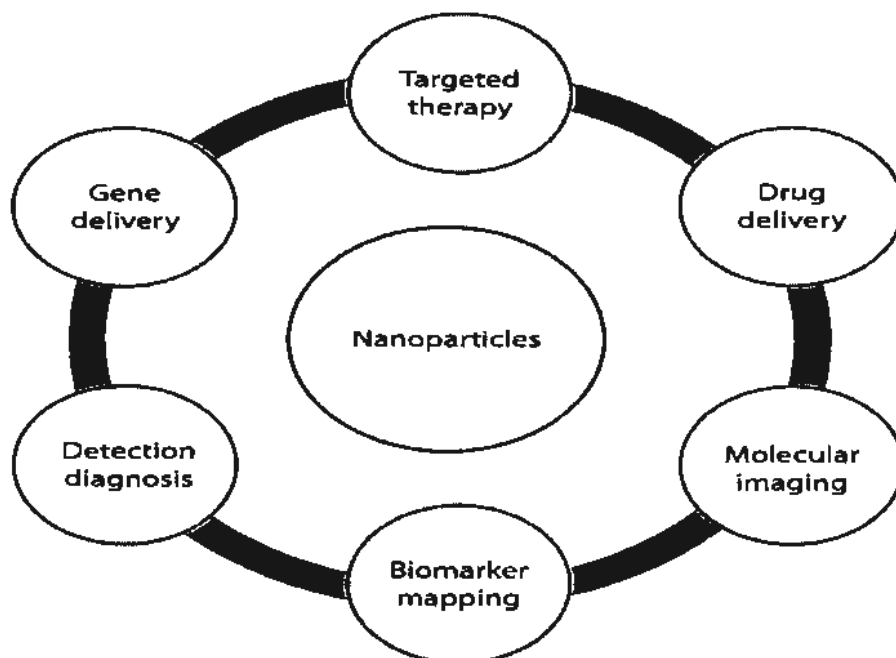
Fig. 1.3: Bio-medical applications of magnetic nanoparticles [8].

The magnetic properties of nanoparticles are dependent upon their size, shape, preparation technique and chemistry of the materials. The most commonly examined magnetic nanomaterials are Nickel, Cobalt, Chromium, Iron compounds and their alloys [9].

1.4   Magnetism and its Concepts

The basis of magnetism is the flow of electric charges. Almost all materials have the ability to respond to the magnetic field lines; however some shows very little magnetic response. Electrons are the origin of magnetism in a single atom and these atoms make the magnetic field of the whole matter. Electrons generates magnetic field due to two types of motion, one is the spin motion which is the quantum mechanical behavior of electron and behaves like tiny bare magnet. The spin motion may be up or down.

The other type of motion is the circulatory motion of electron around the nucleus which is just like the current loop. The magnetic field due to spin motion is stronger than the field produced by spherical motion of electron [10]. The magnetic field lines generated by motion of electron in a circular loop are said to be a dipole [11]. The Fig. 1.4 shows two types of magnetic moments, magnetic moment due to orbital motion of electrons and magnetic moment due to the spin motion of electrons. The electrons orbiting around the nucleus in an atom respond to the external

4

magnetic field in some specific configuration. Electron spin has the prominent magnetic effect in the atom. Magnetic dipoles consist of equal and opposite magnetic moments. The dipole concept is used to describe the basic magnetic quantities. Free moving charges produce field of magnetic field strength (H) [12].
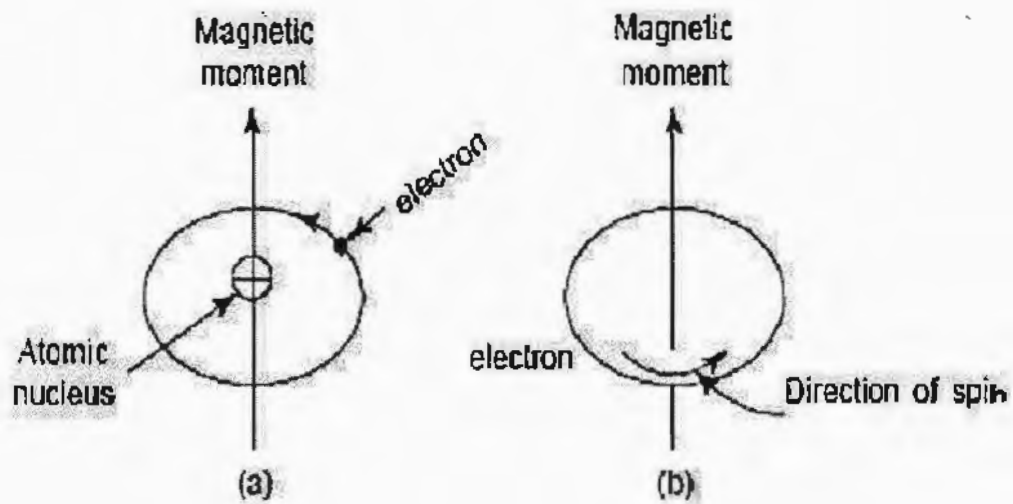
Fig. 1.4: (a) Orbital magnetic moment (b) Spin magnetic moment [13].

Magnetic dipole moment is the vector product of current (I) due to orbital motion of electron and area (A) of circular loop, so dipole moment can be mathematically represented as;

$$M = I \times A \qquad (1.1)$$

Magnetic dipole vector is a vector quantity and its unit is A-m^2. The equation 1.2 represents the direct dependence of external magnetic field on field intensity (H) and the magnetization (M).

$$B = H + 4\pi M \qquad (1.2)$$

The 4π factor in equation 1.2 represents the unit field produced by a unit pole on the surface of a sphere with radius of 1 cm, where the unit polar surrounds the pole with a surface area of 4π cm^2 [14].

Magnetization is also the function of magnetic susceptibility (χ_m) and magnetic field intensity (H), as from Equation 1.3.

$$M = \chi_m H \qquad\qquad (1.3)$$

Where magnetization (M) is the ratio of net dipole moment to volume in the material (Equation 1.4),

$$M = U_{total}/V \qquad\qquad (1.4)$$

Magnetic susceptibility is a dimensionless quantity and it measures the response of a magnetic material to an external magnetic field. Magnetic susceptibility can be expressed in terms of;

$$\chi_m = \mu_r\text{-}1 \qquad\qquad (1.5)$$

Where μ_r is the relative permeability and it shows the degree of magnetization obtained by a material in response to externally applied magnetic field [15].
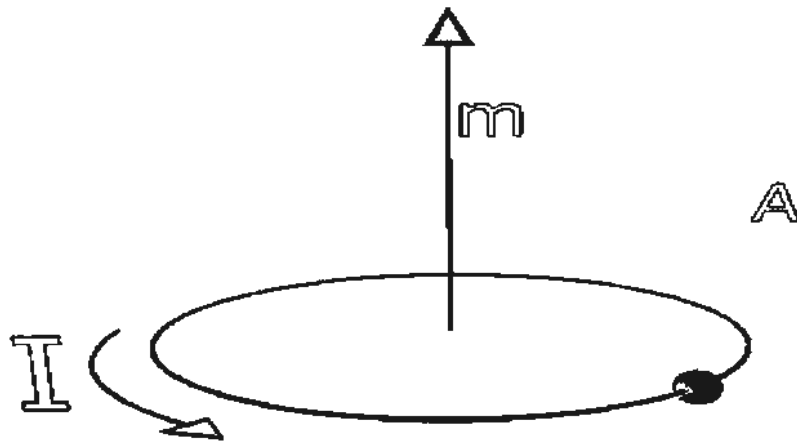
Fig. 1.5: Circulating electron causing dipole moment [13].

The Fig. 1.5 is the representation of direction of current in form of orbital motion of electrons and the magnetic dipole moment. According to right hand rule, the curve fingers points in the direction of current and thumb shows the direction of dipole moment.

1.5   Types of Magnetism

Materials are categorized into different magnetic materials by their response to external magnetic field. The different types of moment alignments in a material help to recognize various kinds of magnetic behaviors observed in nature. There are five different forms of magnetism i.e. diamagnetism, ferromagnetism, paramagnetism,

6

antiferromagnetism and ferrimagnetism. All materials have a diamagnetic element of magnetic behavior.

1.5.1 Diamagnetism

Diamagnetic property is due to the filled orbital shells of atoms where opposite spins cancels the magnetic effect of each other. Hence net magnetization becomes zero due to unavailability of unpaired electrons in outer shells. The atomic magnetic current loops of electrons respond oppositely to an externally applied magnetic field. All those materials which show such kind of weak repulsive force to external magnetic field are known as diamagnetic materials.
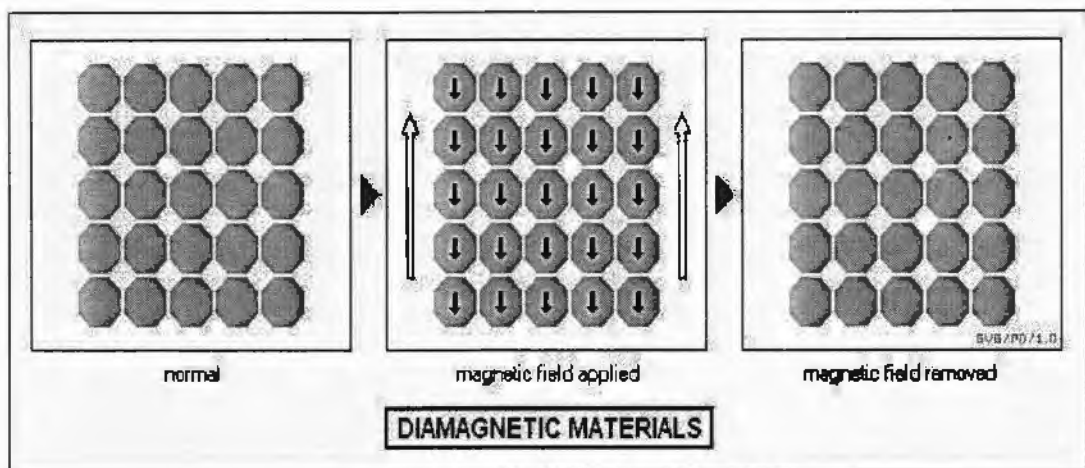
Fig. 1.6: Magnetic field effect in diamagnetic materials [16].

Thermal energy has no effect on diamagnetic property of the materials. The externally applied magnetic field is opposed by induced magnetic moments in diamagnetic materials that cause negative susceptibility ($\chi < 0$). The magnetic behavior of these atomic current loops can also be controlled if the material has long range assembling of magnetic dipole moments [17].

The Fig. 1.6 displays the diamagnetic effects of materials before and after applying the field. Copper, Bismuth, Silver and Gold etc. are the well-known examples of diamagnetic materials.

1.5.2 Paramagnetism

Paramagnetism arises in those types of materials which have unpaired magnetic moments. These magnetic moments are randomly arranged and possess their own magnetic field due to weak spin coupling. This weak spin coupling of a

7

magnetic material is due to thermal energy. The susceptibility of a paramagnetic materials is positive ($\chi > 0$), which means that they are attracted by magnetic field. In an applied external magnetic field, there are maximum number of spins which aligns with the external field, depending on the type of paramagnetic material and strength of the applied field.
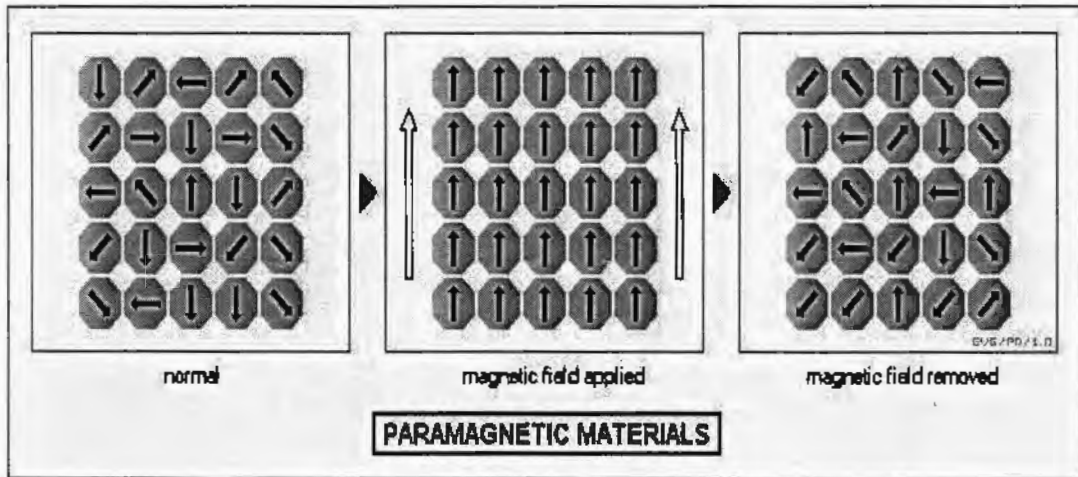
Fig. 1.7: Paramagnetic spin alignments before and after applying magnetic field [18].

Thermal energy of a magnetic material is dominated when field is removed because it randomizes the magnetic spins resulting in no net magnetization. The magnetic dipole moments are easier to align at lower temperatures [13].

The Chromium, Oxygen, Platinum and Aluminum etc. are the examples of paramagnetic materials. The Fig. 1.7 shows the paramagnetic behavior of magnetic dipole moments before and after applying external magnetic field.

1.5.3 Ferromagnetism

Ferromagnetism is the magnetic property of materials which occurs due to spontaneous magnetization even in the absence of external magnetic field. The ferromagnetic materials have long range order of spins, where these spins are oriented in some specific direction below the Curie temperature (T_c). This alignment of spins is strong enough to yield net magnetization in each domain.

There is large number of small magnetic domains in the ferromagnetic materials which contains large number of individual magnetic moments. Each domain is totally magnetized due to parallel ordering of magnetic moments. Domain wall lies in between different magnetic domains which separates the domains from each other.

8
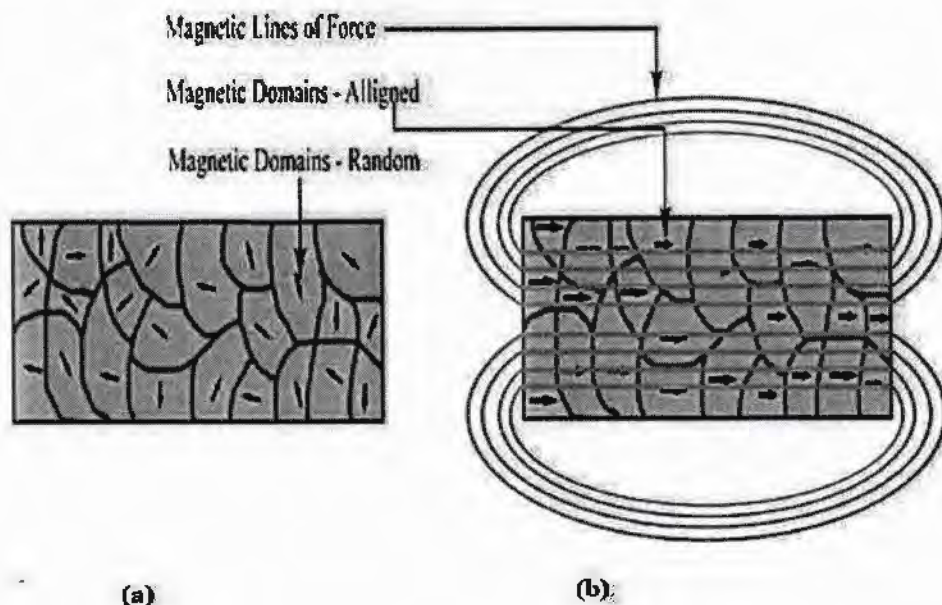
Fig. 1.8: Ferromagnetism (a) in absence of magnetic field (b) in presence of magnetic field [13].

The net magnetic moment of each magnetic domain has different directions in proceeding from one domain to another. Due to random order of net spins of several magnetic domains, the total magnetization of a material become zero [19]. In an applied external field, the magnetic moments of all the domains aligned themselves with the field resulting in a maximum magnetization as displayed in Fig. 1.8.

Ferromagnetic materials are classified into two types of materials known as hard and soft ferromagnetic materials. The hysteresis loop of a hard ferromagnetic material is large and wide even when the applied field is zero. These materials are used in forming permanent magnets. Cobalt steel is the example of a hard ferromagnet material. Soft ferromagnetic materials have smaller hysteresis loops and contain small value of magnetization in the absence of applied field [20]. An example of a soft ferromagnetic material is Silicon steel.

1.5.3.1 Magnetic Anisotropy

Magnetic anisotropy is derived from spin orbit coupling of electrons, which is an inherent characteristic of a magnetic material depending upon the crystallographic alignment of the sample [14]. The dependence on the direction of magnetization was experimentally detected, which specifies the presence of magnetocrystalline anisotropy.

9

The energy related to the orientation of magnetic moments is explained in equation 1.6

$$E_a = K \sin^2\theta \qquad (1.6)$$

In equation 1.6, 'K' is the anisotropy energy constant; 'θ' is the angle between saturation magnetization direction and easy axis. The easy axis of a crystalline material is the preferred direction of the magnetic spins of a given material. The magnetic susceptibility of a material is larger when the saturation magnetization is induced along the easy axis of a crystalline material. Shape anisotropy is produced due to the effect of the induced magnetization on the physical shape of a material and is important for non-spherical materials [21].

1.5.3.2 Hysteresis Loop

When a ferromagnetic or ferrimagnetic material placed in an external magnetic field, the magnetic spins of every domain starts rotating in the direction of field unless all magnetic dipole moments are oriented in the field direction [21]. Magnetization starts reducing when the externally applied field is decreased. During demagnetization process if the demagnetized line does not follow the initial magnetization curve, then material shows hysteresis loop. The highest region of the magnetization loop is the saturation magnetization as indicated in Figure 1.9.
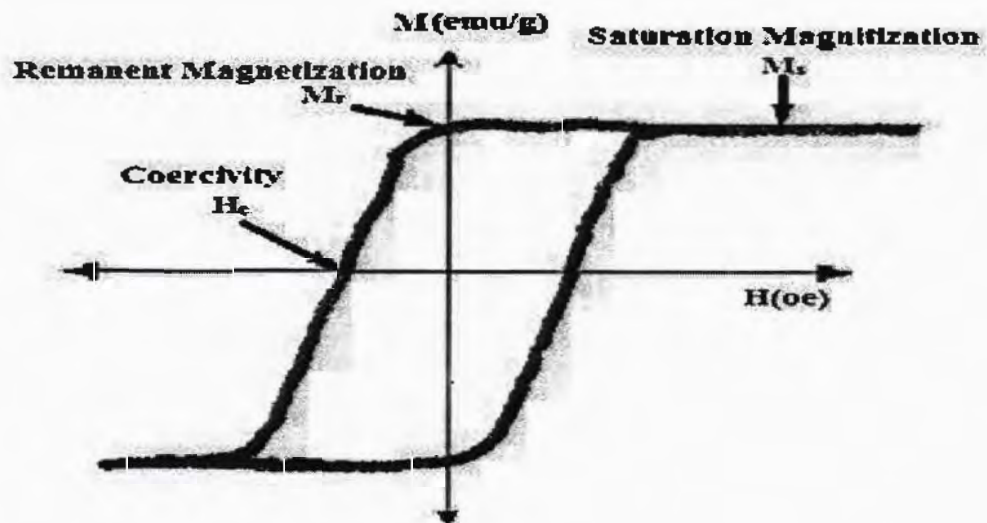
Fig. 1.9: Hysteresis loop of a ferromagnetic material [22].

10

Magnetization at zero applied magnetic field is said to be remanence magnetization (Mr) and when the external magnetic field is applied in the opposite direction to make the net magnetization to zero then it is termed as coercive force (Hc) [16].

1.5.3.3 Magnetic Relaxation

When the magnetic dipoles of a material are placed in the field of a magnet, then there is a period of time for which it relaxes into its equilibrium position. This is named as magnetic relaxation. This process is usually dependent upon magnetic anisotropy in which magnetic moments of a material relaxes more easily in easy axis as compared to the hard axis of the material. It is also dependent on thermal energy. There are usually two different types of relaxations known as Neel's and Brownian's relaxation. Neel's relaxation is the time taken by a single spin flip between its energy minima due to thermal variations in absence of magnetic field. It is measured by using the Neel's Arrhenius law (equation 1.7):

$$\tau = \tau_0 exp\ (E_a/k_BT) \tag{1.7}$$

Where 'τ_0' is the single atomic spin flip time ranges from 10^{-9} s to 10^{-10} s, 'E_a' is the activation energy and 'k_BT' is the thermal energy [23].

1.5.4 Antiferromagnetism

Materials having magnetic spins of equal magnitude but opposite in direction are known as antiferromagnetic materials. The exchange interaction property pairs the magnetic spins in such a way that they are opposite in direction and cancelling the effect of each other leaving zero net magnetization.
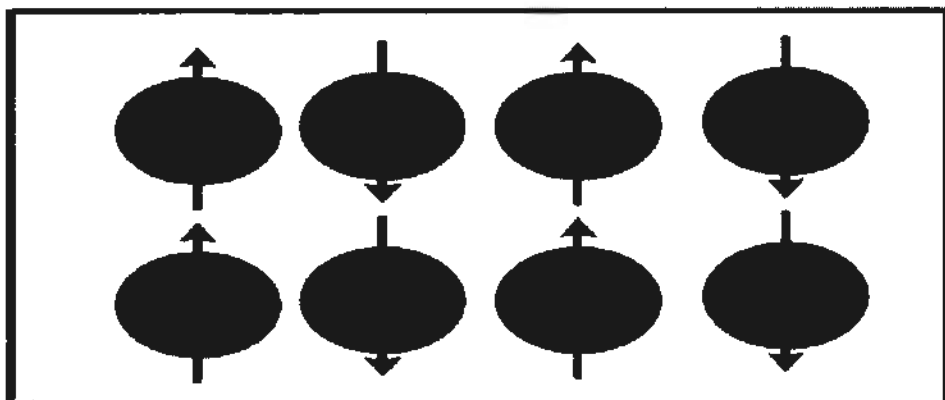
Fig. 1.10: Opposite alignment of spins in an antiferromagnetic material [13].

11

Thermal energy above the Neel's temperature is enough to cause the equal and antiparallel arranged magnetic spins to thermally oscillate and leading to break their long range spin order. Where in this state, a magnetic material displays paramagnetic property [21]. The Fig. 1.10 indicates the antiparallel arrangement of magnetic spins in an antiferromagnetic material.

1.5.5 Ferrimagnetism

Ferrimagnetism has some resemblances to antiferromagnetism, where the pairs of sub lattice spins in a crystalline material is antiparallel having magnetic spins of unequal magnitudes. This difference results in net magnetization which is indicated in Fig. 1.11. Both ferrimagnetism and antiferromagnetism were discovered by Louis Neel [24]. The ferrimagnetic behavior of a material is also dependent upon transition temperature known as Neel temperature (T_N). On increasing the thermal energy of the material, the long range spin structure of the magnetic material breaks into small chains and dispersed in random order, where material becomes paramagnetic.
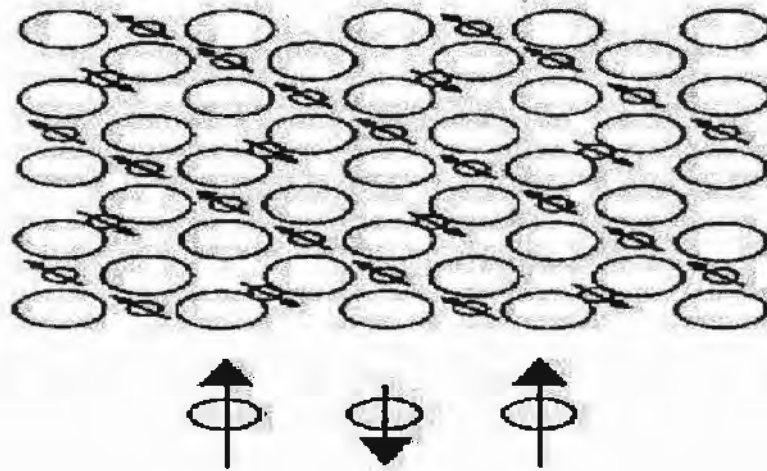
Fig. 1.11: Ferrimagnetic behavior with antiparallel and unequal magnetic spins [17].

1.6   Ferrites

Ferrites are famous composites in the form of ceramic material in which iron oxide is the elementary component. Ferrites (ferrimagnetic materials) belong to the class of ferrimagnetism. The structural formula of ferrites is AB_2O_4, in which A denotes the divalent metal ions such as Mg^{+2}, Co^{+2}, Fe^{+2}, Ca^{+2}, Cu^{+2} and B indicates trivalent cations like Fe^{3+} and Al^{3+} [13]. Ferrites are categorized into two groups on the basis of their different magnetic behaviors named as soft and hard ferrites.

12

1.6.1 Soft Ferrites

Soft ferrimagnetic materials have low coercivity and small hysteresis loops. These are ferrimagnetic in nature having cubic crystalline structure. Soft ferrites are denoted by the chemical formula $MOFe_2O_3$, where M represents the group of transition metals i.e. Iron, Manganese, Cobalt and Zinc. These materials can be easily magnetized and demagnetized. The motion of domain wall occurs easily in a soft ferrimagnetic material which is accredited to proper annealing, surface impurities and dislocations [25].

1.6.2 Hard Ferrites

Hard ferrites belong to the class of those materials which have large value of coercivity and remanence magnetization. Hard ferrimagnetic materials composed of compounds of Barium, Iron and Strontium oxide etc. When hard ferrites are magnetically saturated, then permeability of these magnetic materials is increased as well as conductive properties are also enhanced. So the capability to accumulate powerful magnetic field of these ferrimagnetic materials improves as compared to Iron metal alone. These magnetic materials are significant due to widespread applications of these ceramic materials in house hold appliances like in air-condition coolers etc. [13].

1.7 Spinel Ferrites and their Types

Spinel ferrite materials have cubical structures with small eddy current loss and lower value of resistivity at microwave frequencies [26]. They are ideal for use due to above stated significant properties. Spinel ferrites have chemical formula KFe_2O_3, in which K shows the divalent element comprising of Nickel, Magnesium, Iron, Cadmium, Cobalt and Zinc.

Spinel ferrites have close packed structure with 32 oxygen ions making unit cell and usually show FCC crystal structure. There are two interstitials positions which can be filled by metallic ions. Tetrahedral lattice site (A) and octahedral lattice site (B) for divalent and trivalent iron cations are present. There are 64 tetrahedral and 32 octahedral lattice sites are available in a unite cell of spinel ferrite structure which is shown in Fig. 1.12 [27].

13
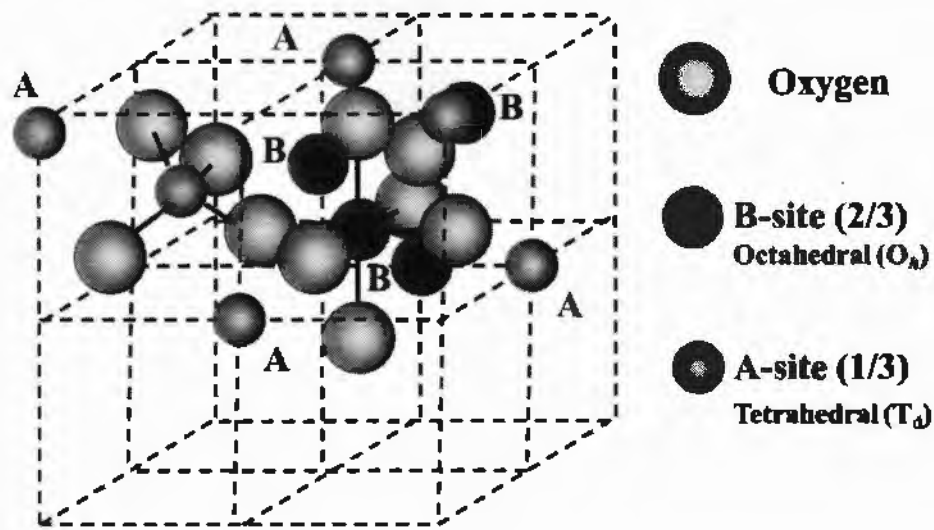
Fig. 1.12: Unit cell of spinel ferrite having octahedral (B) and tetrahedral (A) lattice sites [28].

Spinel ferrites based on crystal structure are categorized into following three classes,

1. Normal spinel ferrites
2. Mixed (intermediate) spinel ferrites
3. Inverse spinel ferrites

1.7.1 Normal Spinel Ferrites

Normal spinel ferrite structures have one type of metallic cations on tetrahedral and octahedral lattice sites. Divalent cations are present tetrahedral lattice sites whereas trivalent cations occupy octahedral lattice sites. Metallic ions reside on total 8 tetrahedral and 16 octahedral sites. Formula of normal spinel ferrite is $[D^{2+}]_A[Dv^{3+}]_BO_4$, where D and Dv represent divalent and trivalent cations respectively. The example of normal spinel ferrites is bulk Zinc ferrite [29].

1.7.2 Mixed Spinel Ferrites

Mixed spinel ferrites are also termed as intermediate spinel ferrites, as there ionic distribution lies in between normal and inverse spinel ferrites. The compositional formula is $[D\delta^{2+}Dv_{1-\delta}^{3+}]_A [D_{1-\delta}^{2+}Dv_{1+\delta}^{3+}]_BO_4$, in which D and Dv indicates the divalent and trivalent lattice sites whereas δ expresses inversion parameter. Usually, for normal and complete spinel ferrites, the values of inversion parameters are 1 and 0 respectively. The uneven distribution of cations on octahedral sites also represents the class of mixed spinel ferrites [30]. Manganese ferrite

14

($MnFe_2O_4$) and Magnesium ferrite ($MgFe_2O_4$) are examples of intermediate spinel ferrites.

1.7.3 Inverse Spinel Ferrites

Inverse spinel ferrites are known by distribution of half trivalent ions on octahedral lattice sites (B) while reaming half on tetrahedral lattice sites (A). Inverse spinel ferrites are represented by general formula $[Dv^{3+}]_A [D^{2+}Dv^{3+}]_B O_4$, where D and Dv denotes divalent and trivalent cations individually. Magnetite (Fe_3O_4) is an example of inverse spinel ferrite materials in which iron ion occupy octahedral lattice site [29].

1.8   Applications of Ferrites

Ferrites are metallic oxide materials with semiconducting property. These materials have great technological significance attributed to their remarkable electrical and magnetic behaviors. Ferrites have applications in transformer cores, microwave oven, antenna rods, magnetic data storage devices, permanent magnets, magnetic recording media, transducers, activators and computer memory chips [31].

The ferrites in nanocrystalline structure are used in different fields i.e. targeted drug delivery, catalyst, gas sensors, magnetic ferro-fluids and biotechnology [32]. Ferrimagnetic materials have wide applications in high frequency devices on behalf of their minimum cost, high resistivity and small loss of eddy current. The crystalline ferrites can't be replaced by any other magnetic materials due to their key role in industrial applications. That is why, the processing of these materials is important in changing the properties for desired applications [33].

1.9   Iron Oxides and their Applications

Iron oxides are chemical compounds of iron and oxygen. Iron oxides occur in different form of chemical compositions having different magnetic properties. There are almost sixteen types of iron oxides and oxyhydroxides [34]. Iron oxides are interesting materials to magnetically guidable systems. These oxides include the maghemite, magnetite and $MO.Fe_2O_3$ (M= Mn, Co, Ni, Cu). These materials show ferrimagnetic nature. Ferrimagnetic iron oxides are less affected by magnetic field as compared to ferromagnetic materials. The lower magnetic response of iron oxide composites is attributed to less sensitivity in oxidation process [35].

Common types of iron oxides:

1) Iron(+2) oxide, wüstite (FeO)
2) Iron(+2, +3) oxide, magnetite (Fe_3O_4)
3) Iron(+3) oxide (Fe_2O_3)
    1. alpha phase, hematite (α-Fe_2O_3)
    2. beta phase, iron (+2) oxide (β-Fe_2O_3)
    3. gamma phase, maghemite (γ-Fe_2O_3)
    4. epsilon phase, iron (+2) oxide (ϵ-Fe_2O_3)

(a) Hematite　　　**(b) Magnetite**　　　**(c) Maghemite**
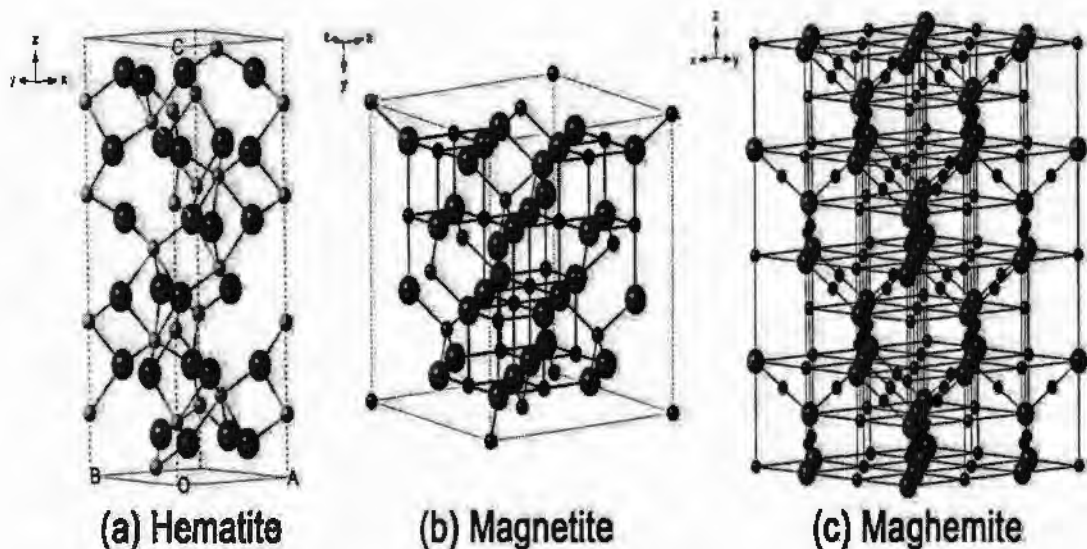
Fig. 1.13: Crystal structure of the hematite, magnetite and maghemite (the small ball is Fe^{+2}, the medium ball is Fe^{+3} and the big ball is O^{-2}) [36].

There are different types of iron oxides having different crystallographic structures, such as rhombohedral hematite, cubic magnetite and tetragonal maghemite which are indicated in Fig. 1.13. Maghemite and magnetite are the most commonly researched iron oxides. The mixed metal (MO·Fe_2O_3) iron oxides have different physical and magnetic properties, which are commonly used for electronics applications due to the single domain nature. Magnetite and maghemite have same physical properties and crystalline structure. Both type of iron oxides show ferrimagnetic behavior. The only change in their magnetic response to an applied magnetic field is accredited to sub lattice interactions [37].

Superparamagnetic iron oxide nanoparticles have found wide range of technological applications in magnetic storage data devices, biosensing, medical uses

16

like directed drug supply, magnetic resonance imaging (MRI) and magnetic inks for jet printing [38]. Iron oxide nanoparticles with proper surface chemistry is usually used in biological tissue repairing, immunoassay, purification of biological fluids, magnetic hyperthermia, MRI contrast developed drug delivery and cell parting [39]. Altogether these biomedical applications of iron oxide nanoparticles need high magnetization values, small sizes and narrow particle size distribution.

1.10   Structure of Zirconia (ZrO_2) and its Applications

Zirconia (ZrO_2) is a sparkly white-gray metal, which looks like blue-black in powder form. ZrO_2 is an oxide of zirconium having high ductility, maximum hardness, resistance to rusting and malleability. ZrO_2 is not found in pure form in nature, therefore it requires hard processing to get pure ZrO_2 [40]. Pure ZrO_2 shows monoclinic crystalline structure at room temperature. Although, the crystalline powder of ZrO_2 can be refined and purified chemically at higher temperatures, making a cubic crystal structure known as cubic zirconia, which is indicated in Fig. 1.14.
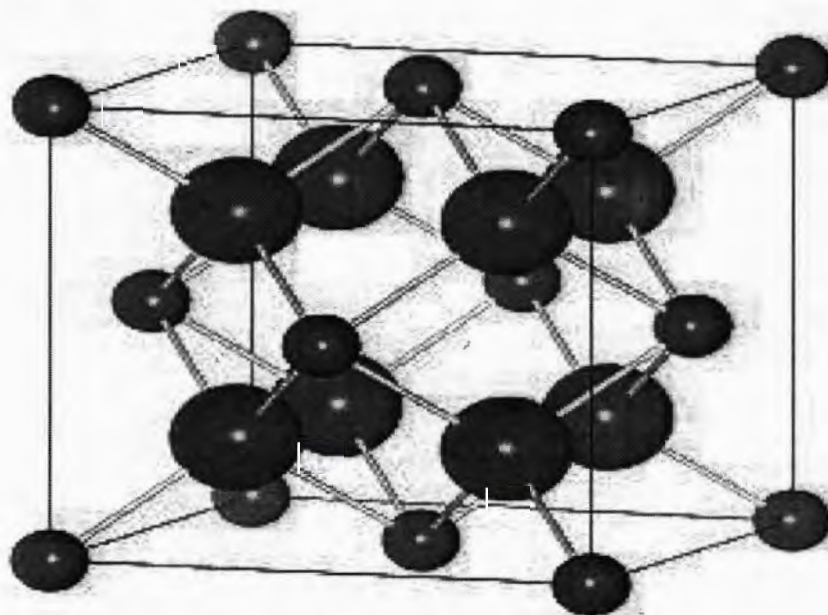
Fig. 1.14: Cubic unit cell of ZrO_2 composing of oxygen (large balls) and iron (small balls) [41].

The ZrO_2 material is tough, optically sound and transparent, typically used for forming valuable stones and gas sensors [42]. The three-dimensional arrangement of the atoms in ZrO_2 is normally represented by different crystallographic structures,

17

showing the property of polymorphism. ZrO_2 has three crystal forms namely monoclinic, tetragonal and cubic, which are usually analyzed by definite geometry and structural factors [43]. ZrO_2 is emerging as an adaptable and promising material among the dental ceramics due to its biological and mechanical properties. ZrO_2 based ceramics have extensive uses in structural engineering, for example in making cutting tools, gas sensors and refractories [44].

1.11 Effects of Surface Coating on Maghemite Nanoparticles

Maghemite (γ-Fe_2O_3) nanoparticles possess large surface area to volume ratio and hence keep high surface energies. These particles tend to agglomerate with each other in order to reduce their surface energies. The agglomeration is the effect of accumulative forces between the nanoparticles, which includes the van der Waals forces and dipole-dipole interactions [45].

Likewise, the bare maghemite nanoparticles have high chemical reactivity and can be easily corroded in air (particularly magnetite). These particles usually causes in loss of magnetic property and dispersive property of nanoparticles. Consequently, it is very necessary to maintain the stability of magnetic maghemite nanoparticles by adopting specific effective protection strategies and suitable surface coating. These strategies consist of embedding or coating with organic molecules like polymers, proteins, biomolecules, or surface coating with an inorganic material i.e. metal oxide, metal sulfide and nonmetal substances. Metal oxide coating includes zirconia, silica and aluminum oxide etc.

Superparamagnetic maghemite nanoparticles can also be stabilized in solution by electrostatic repulsive forces. Particularly, in most cases, coating with metal oxide not only stabilizes the maghemite nanoparticles, but also utilized for further functionalization [46]. ZrO_2 was chosen as a coating material, as it is not only good insulating material but also has other interesting properties like chemical passiveness, high resistance and fracture stiffness etc.

1.12 Superparamagnetism

The magnetic anisotropy which keeps the magnetic particles aligned in particular direction, is normally dependent on the volume of the particles [47]. As the particle size reduces, the energy related with the uniaxial anisotropy also reduces

18

unless thermal energy is enough to overcome the preferred alignments of magnetic moments in a magnetic domain. A single magnetic domain particle that acquires balance magnetization at experimental temperatures in short times comparative to the measurement time is generally known as superparamagnetic [48].
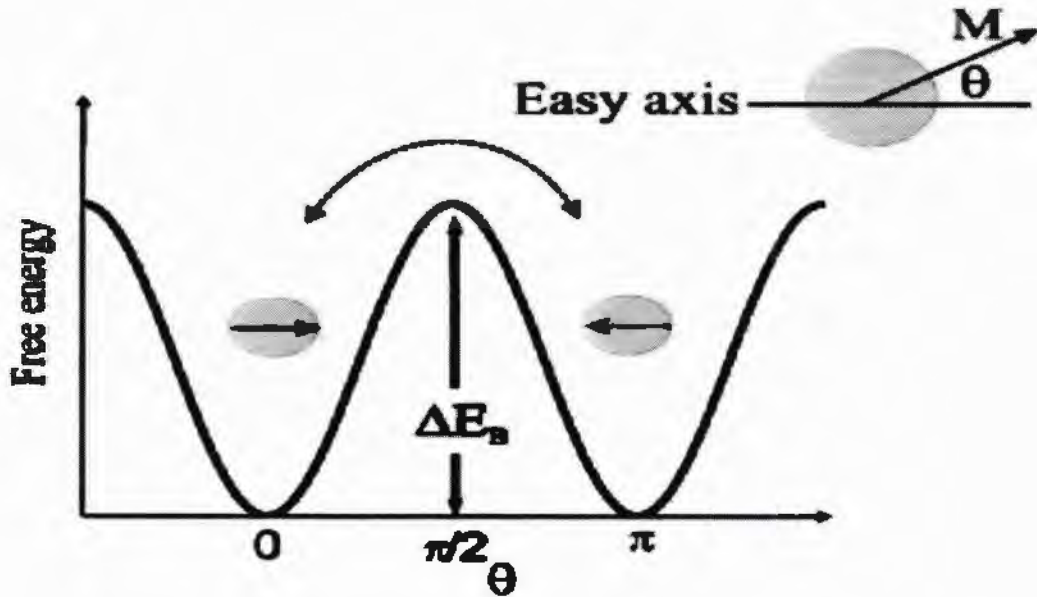
Fig. 1.15: Blocked and superparamagnetic state of a nanoparticle [17].

On the other hand, system develops multi domain structure at larger particle sizes, where domain walls become dominant. Superparamagnetic particles depend on magnetic anisotropy, which means that the electron magnetic moments directed in "easy axis" leads to high values of magnetization in that preferred direction. This magnetic anisotropy is due to the particle size, shape and stress. The Fig. 1.15 demonstrates the superparamagnetism process having anisotropy energy barrier in between the two easy axis of a single domain particle [49].

CHAPTER 2

Literature Review

In this section, we present the analysis of the work which has been researched and analyzed by several researchers on the preparation and characterization of maghemite nanoparticles. There is special focus on the work published on magnetic studies of ferrites; mainly on the iron, manganese and copper ferrites and mixed spinel ferrites. The biomedical and technological applications of these spinel ferrites have also been discussed in detail. The analysis of maghemite will assist the reader to acquire the knowledge about the significance of work; we have done in the current study. The properties of superparamagnetic maghemite nanoparticles are significantly affected by the physical properties of the powder such as size, shape, pureness and chemical structure of the particle.

Kodama *et al.* [50] have studied the magnetic properties of iron oxide nanoparticles. These nanoparticles have shown distinct physical and chemical behaviors like superparamagnetism and these magnetic nanoparticles can also be carried to a particular spot by applying external magnetic field. A magnetic particle is composed of merely one particular magnetic domain below a critical diameter which is almost 5-20 nm for maghemite (γ-Fe_2O_3) and magnetite (Fe_3O_4) particles [39], so these nanoparticles are at the state of constant magnetization at any magnetic field in a fine dispersed medium without any interaction with adjacent domains. Material consist of these magnetic nanoparticles shows magnetic properties in an applied magnetic field, but in absence of field, magnetic behavior vanishes [51]. The cause for this behavior is termed as superparamagnetism, in which the magnetic domains will undergo frustration behavior by having sufficient space to refuse the agglomeration of nanoparticles.

Sheng-Nan *et al.* [52] reported that superparamagnetic iron oxide nanoparticles are the most common nanoparticles which have uses in biomedical field and this is attributed to small cost of synthesis, low toxicity and distinct magnetic behavior. Magnetite and maghemite phases of iron oxide have been broadly investigated on the basis of their synthesis methods, magnetic characterizations,

20

surface variations and biomedical applications. Iron oxide nanoparticles generally display superparamagnetic behaviors when their sizes become less than 20 nm and these are named as superparamagnetic iron oxide nanoparticles. This article provides brief introduction about iron oxide nanoparticles on the basis of their magnetic applications such as targeted drug delivery. it also gives information about fabrication techniques, surface protection strategies and application examples from current important literature. The surface coating and size of nanoparticles have key roles in biomedical uses. The author analysis concentrates on the fabrication methods and surface variations of superparamagnetic iron oxide nanoparticles.

Wu *et al.* [53] analyzed surface modified superparamagnetic iron oxide nanoparticles, which are unique efficient materials having wide applications in the field of catalysis and biotechnology. This article emphasis on current improvement and numerous different approaches in synthesis, assembly and magnetic characteristics of bare and surface coated magnetic iron oxide nanoparticles. These nanoparticles have observed behaviors of high saturation magnetization, surface stability, biocompatibility and interactive magnetic properties at surface in order to implement the useful applications. Furthermore, iron oxide nanoparticles surface can be changed by coating with organic material or inorganic material i.e. polymers, biomolecules, zirconia and nonmetals etc. There is special focus on complications and challenges related to the preparation and surface coating of iron oxide nanoparticles. Moreover, multifunctional magnetic iron oxide merged nanoparticle designed with dynamic sites will promise for numerous potential uses like catalysis, magnetic recording media, bio-separation and bio-detection, etc.

Chirita *et al.* [54] examined the key properties of iron oxide nanoparticles and their numerous photo-electrochemical uses. Several different innovative methods are described in the application of photo-electrochemistry, like solar energy conversion, water splitting and photo-catalysts for purification of aqueous or gas phases of a material by removing the organic and inorganic particles. Sometimes, these applications in some specific surroundings require the surface variation of nanoparticles in order to shield them from chemical frustration and aggregation. The surface coating can also be used to enhance the functionalities of the magnetic core, for instance biological stealth, optical properties, catalytic and adsorbing ability.

21

Nadeem *et al.* [55] analyzed the effects of surface spins on magnetic characteristics of maghemite nanoparticles having 6 nm size. The magnetic properties have been studied by using SQUID analysis and also these experimental outcomes were compared with theoretical models. Magnetic moments surface frustration generated in maghemite nanoparticles is attributed to surface disorder of magnetic dipole moments. The theoretical simulation of ac-susceptibility has been used to study the new results of ac-susceptibility. When the experimental and theoretical results are compared, then it results in the existence of large active anisotropy and freezing surface effects of magnetic iron oxide nanoparticles. These different effects are due to an enhanced toughness of frozen surface moments which obeys the dynamic scaling law. This law is different from Arrhenius law. The effective anisotropy constant (K) of these maghemite nanoparticles is increased as compared to bulk maghemite, which is accredited to the occurrence of randomly arranged surface spins.

Islam *et al.* [56] synthesized unique neck structured hematite, maghemite and magnetite nanoparticles by modified hydrothermal technique. The X-ray structural analysis has shown the purity of the magnetic nanoparticle. All the products were analyzed through transmission electron microscope to find the shape and size of nanoparticles. Neck structured particles shape was detected for the first time among all superparamagnetic iron oxide nanoparticles. The size of particle lies in between range of 50 to 60 nm. The SQUID analysis of magnetic nanoparticles has shown excellent values of magnetization and hysteresis loops. Likewise, the as-synthesized nanomaterials suspensions displayed the temperature rise in the applied AC magnetic field which specifies the possibility of hyperthermia.

Nadeem *et al.* [57] have examined the effects of spin and exchange interactions on magnetic behaviors of maghemite nanoparticles, which are synthesized through microwave plasma method. The transmission electron microscopy and zero field cooled measurements of as-synthesized nanoparticles indicate highly mono-disperse size distribution of nanoparticles with small value of blocking temperature. The experimental readings of these mono-dispersed magnetic nanoparticles are quantitatively compared with theoretical models. The existence of high coercivity and wide hysteresis loops at high magnetic field (75 T) is because of large surface area. Simulated and experimental FC-ZFC models display difference in their field cooled (FC) curves which is attribute to non- interacting single-domain

22

magnetic particles. Effective anisotropy constant results in greater value than the analogous bulk value due to an extra influence of magnetic anisotropy. Fitting of Arrhenius law provides unreasonable values of activation energy parameter and atomic spin flip time. Fitting of Vogel–Fulcher law gives reasonable results of fitting parameters. The increase of the interaction parameter (T_0) is accredited to stronger interparticle interactions. Dynamic scaling law fitting is used to check the spin-glass freezing effect. Maghemite nanoparticles produce reasonable results of critical exponent parameter which shows the presence of surface spin glass freezing effect. Coercivity is enhanced in maghemite nanoparticles due to the existence large magnetic dipolar interactions.

Osborne et al. [58] studied a fast, direct microwave plasma assisted preparation of dextran surface coated iron oxide nanoparticles. The nanoparticles were synthesized in two hydrodynamic magnitudes with varying core shell structures, which were done by changing the technique as either a two-phase or single phase procedure. The remarkable advantage of this technique is to get rapid and reliable results without the need of PH or temperature sensitive methods. Microwave plasma preparation of superparamagnetic iron oxide nanoparticles offers opportunities for quick production of clinically related contrast agents and the ability to discover new platforms for future magnetic resonance contrast agents with almost immediate results.

Nadeem et al. [59] have analyzed the magnetic properties of maghemite (6nm) nanoparticles with the help of SQUID analysis. Superparamagnetic maghemite nanoparticles have been synthesized by microwave plasma method which is used to avoid the aggregation of nanoparticles. Magnetization curves of ZFC-FC indicate blocking temperature value at 75 K. Fitting of Arrhenius law produces unreasonable values of activation energy parameter and atomic spin flip time. AC susceptibility fitted to Dynamic scaling law displays suitable value of critical exponent (zv =10), which should lie in range of 4 to 12 where this value is distinctive for spin glass phase. There is rapid enhancement in temperature dependent coercivity at lower temperature values which is attributed to canted surface spins. Magnetic memory effects and thermo-remanent magnetic behaviors also support the presence of spin glass property. All these magnetization processes indicate the existence of magnetic blockings and spin glass freezing effects at different temperatures.

Deng *et al.* [60] synthesized magnetite (Fe_3O_4) nanoparticles embedded in silica matrix by sol gel technique. The results have shown that the reaction parameters like type of alcohol and the quantity of aqueous ammonia has significant effects on the preparation of silica coated magnetite nanoparticles. The morphology and crystalline structure of silica coated magnetite nanoparticles attain an irregular shape with the increasing of polarity of alcohol, also poor coating efficiency was obtained by using methanol. Magnetite nanoparticles coated with silica matrix were obtained with good morphology and phase structure having volume range from 2 to 4 nm. The quantity of catalyst (aqueous ammonia) plays significant role in the synthesis of nanoparticles. Large magnetite embedded in silica matrix nanoparticles with more proper shape and mono-dispersed nature could be achieved by increasing the quantity of precursor. Magnetic characterization indicates the superparamagnetic behavior of silica coated magnetite nanoparticles.

Benitez *et al.* [61] analyzed the joint structural and magneto-metric properties of self-assembled superparamagnetic iron oxide nanoparticle. These mono-dispersed magnetic nanoparticles were prepared by thermal decomposition route. XRD analysis and transmission electron microscopy were used to characterize the structural and phase properties of iron oxide nanoparticles. These structural and phase characterizations were compared to the magnetic behavior of nanoparticles examined by SQUID analysis.

Zhang *et al.* [62] reported that zirconia based materials are being extensively used as a thermal barrier coating material because of their higher melting temperature and lower thermal conductivity. Structural properties like phase study, density of states, lattice parameter and surface impurities for both monoclinic and tetragonal zirconium dioxide were analyzed. Phase transition of a pressure based tetragonal zirconium dioxide was also found which is based on tetragonal variation and band assembly under compressive forces. The results showed change of monoclinic phase to cubic phase at an applied pressure of 37 GPa. Furthermore, monoclinic zirconia thermodynamic results were also calculated.

CHAPTER 3

Synthesis and Characterization Techniques

3.1 Techniques to Synthesize Nanomaterials

In order to explore unique physical properties and to realize the dynamic uses of nanomaterials, it is the corner stone in nanotechnology to synthesize and process nanomaterials and nanostructures. It has become very essential for the application of nanomaterials with strict control over shape, morphology and size distribution of nanoparticles, moreover, these nanomaterials has wide applications in different fields of nanotechnology i.e. catalysis, biomedicine and solar technology. The performance of nanomaterials is dependent upon their physical properties, which in turn relay on the molecular morphology, configuration, micro-structure, imperfections and surface chemistry of nanomaterials. These properties can be controlled by thermodynamics of the formation of nanomaterials [63]. Preparation of nanoparticles is usually carried out by two different broad categorized methods. First one is top down and another one is bottom up approach. These two approaches are discussed in detail.

3.1.1 Top down Approach

Top down procedure includes the division of the bulk material into nano-sized particles. Top down preparation methods are extension of those techniques which have been applied for production small size particles. This approach of synthesis is simple and dependent on either elimination or miniaturization of bulk material. It is also composed of bulk synthesis methods to obtain the required shape and morphology of nanomaterials. At the nanoscale, top down techniques are normally not fit for fabrication of nanoparticles because these methods currently face technical limitations as well as need tremendously lengthy and expensive procedures [64, 65].

Top down approach includes;

1. Sputtering
2. Laser ablation method
3. Electron beam lithography
4. Plasma etching

The fig. 3.1 shows the two opposite approaches of nanoparticles preparation.
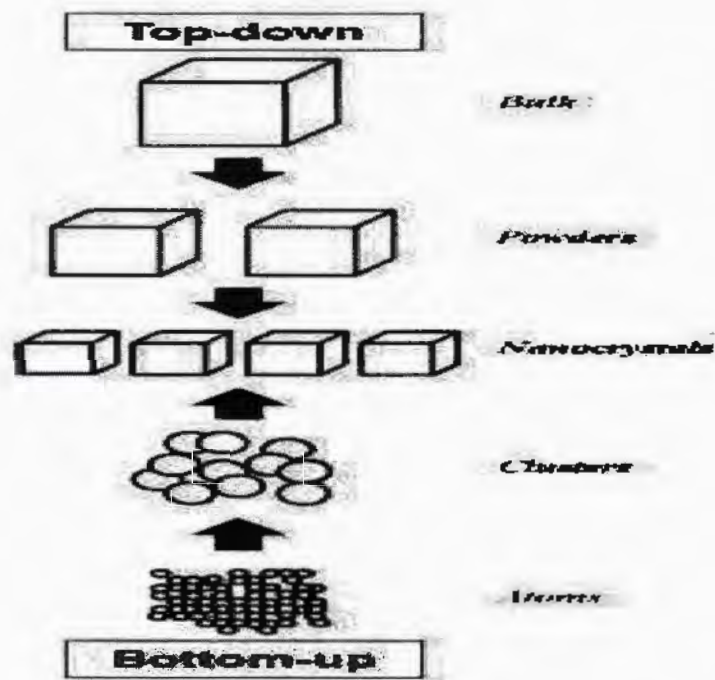
Fig. 3.1: Top down and bottom approach of nanoparticles synthesis [48].

3.1.2 Bottom up Approach

Bottom up approach is composed on the synthesis of nanomaterials from the bottom, where atoms and molecules combine with each other thermodynamically forming new shapes of nanomaterials. This synthesis technique has the potential of producing more pure and less costly materials. Bottom up approach is usually focused in nanotechnology field due to simple preparation procedure, quick synthesis ability and cost effectiveness.

Bottom up techniques are primarily driven by decrease in Gibbs free energy, where the nanomaterial formed is in state closer to thermodynamic equilibrium state. Bottom up methods are one of the easiest, economical and innovative as compared to top down techniques [63, 65].

Bottom up approach involves;

1. Chemical vapor deposition
2. Sol gel method
3. Electrodeposition
4. Microwave plasma method

26

3.2 Preparation of Maghemite Nanoparticles

There are different techniques to synthesize maghemite nanoparticles. Their different structural parameters like structure, size and surface morphology of nanoparticles can be controlled by different procedures, therefore every technique have its own limitations and delimitations as well as advantages and disadvantages [45, 66-68]. Some techniques for the preparation of ferrite and maghemite nanoparticles are mentioned below;

1. Sol gel method
2. Coprecipitation method
3. Hydrothermal synthesis
4. Microwave plasma method

3.2.1 Microwave Plasma Method

Maghemite nanoparticles coated with ZrO_2 have been synthesized by microwave plasma technique [69, 70]. Microwave plasma preparation technique is used to produce highly dispersed nanoparticles with very small particle size distribution. In Microwave plasma preparation method, precursor materials are reacted in the form of gas. Such type of methods is usually operated at low temperatures because plasma produced there is enough for nucleation and growth of nanoparticles. Plasma is the ionized state of matter having zero total charge. Plasma has conductive nature which is attributed to movable charge ions. Fine particles made by microwave plasma method do not interact with each other and avoid aggregation, which is due to surface coating [71, 72].

In the begging of microwave plasma method, the reactant material in the form of liquid or solid is introduced into the microwave plasma system. Here Argon gas is used as a carrier which carries the precursor material in vapor form into plasma region. A precise amount of reaction gas, usually 20% of Oxygen in Argon is injected into the reaction unit exactly in front of microwave plasma zone, where nanoparticles are produced. Another evaporation source facility is also available for the surface coating of nanoparticles.

Now after processing and fabrication of nanoparticles in the microwave discharge region, the argon gas carry nanoparticles with itself passing through the

27

glass tube equipped with water cold glass-finger. The cold glass-finger is situated inside of the glass tub. The cold glass-finger is used for preparation of nanoparticles in dry powder form. When these prepared nanoparticles pass through the tube, they become condense and attach on the surface of cold glass-finger. After formation of nanoparticles, the cold glass-finger having surface accumulation of nanoparticles is removed from the glass chamber and then nanoparticles are collected in the form of dry powder [73, 74].

Iron pentacarbonyl ($Fe(CO)_5$) is used as a reactant material for the preparation of maghemite nanoparticles. A combination of 80% argon and 20% oxygen gas is used as a reaction gas. In this technique, precursor material consuming rate is 15 ml/h and reaction gas flow rate is about 5l/min. The flow rate of Argon gas is noted to be 0.4l/min and total pressure is adjusted at 8 mbar. In microwave plasma process frequency of 2.45 GHz and power 150 W is being used. The temperature is measured to be 200°C after microwave plasma process [71, 74]. The Fig. 3.2 shows the synthesis procedure and steps in the formation of ZrO_2 coated maghemite nanoparticles.
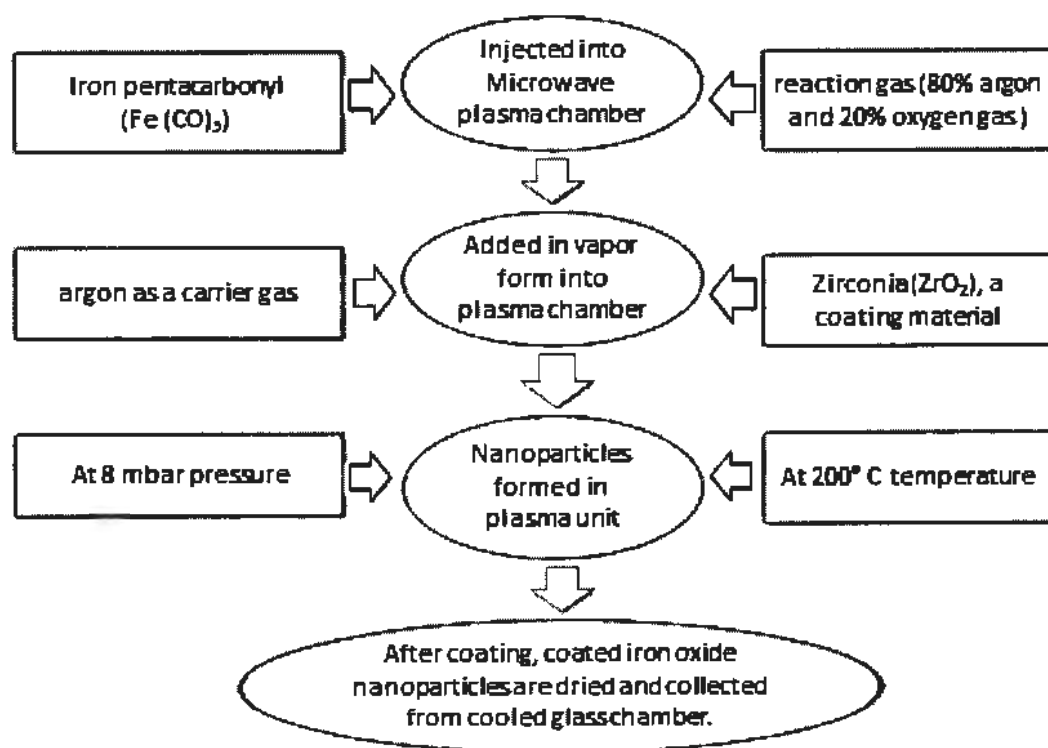
Fig. 3.2: Flow chart of synthesis of ZrO_2 coated maghemite nanoparticles.

28

3.3   Characterization Techniques

There are different characterization methods which are used to characterize the physical properties of maghemite nanoparticles. We can acquire information about structural geometry, surface chemistry, size, shape and internal bonding nature of the nanoparticles with the help of these characterization techniques. Here, we have used XRD for the structural analysis and SQUID magnetometer to study the magnetic properties of ZrO_2 coated maghemite nanoparticles.

3.4   X-rays and their Production

X-rays are a type of electromagnetic radiations having high energy and very small wave length. These rays have the ability to penetrate solids, dense and opaque materials. Their wavelengths are shorter than light and in the range of 0.1 nm to 10nm. German scientist Roentgen had discovered the X-rays in 1895. These rays were named X-rays because of unidentified nature [75]. X-rays are created when a heavy material like tungsten is targeted by fast moving electrons. Fig. 3.3 represents the experimental system of X-rays production in Coolidge tube.
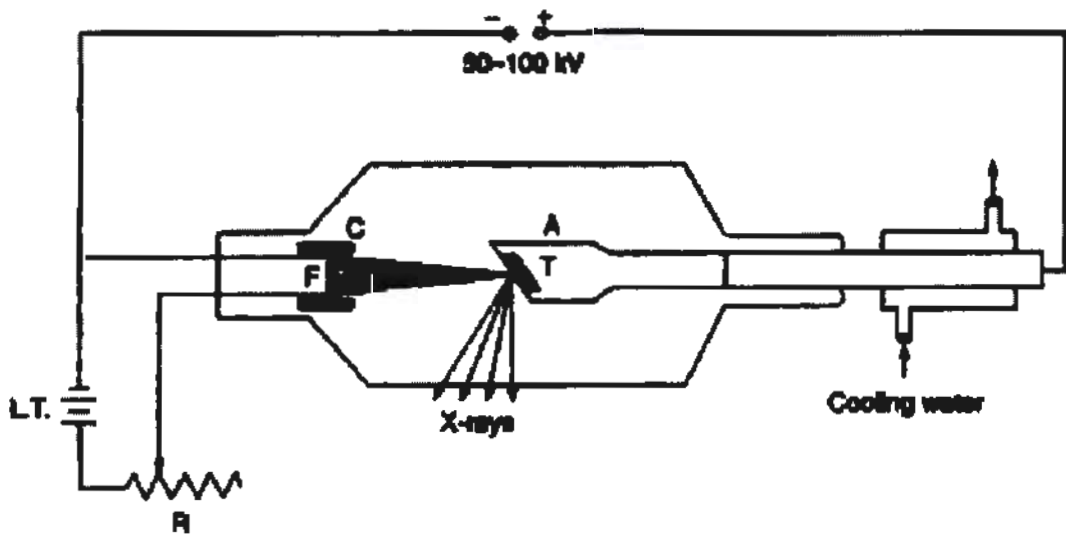
Fig. 3.3: Schematic diagram of X-ray production in Coolidge tube [76].

Coolidge tube is partially evacuated solid crystal cylinder enclosed by lead box. There is thermionic discharge of electrons from the cathode filament by applying low tension supply to the filament. Electrons are focused on the target material with the help of hollow metallic tube 'C'. These electrons are accelerated between anode

29

and cathode filaments by applying high voltage. The accelerated electrons are targeted on the anode 'T' with the help of cylinder 'C'.

Approximately 99.8 % electrons are used in heating the target material 'T' and remaining 0.2% electrons penetrate into the surface of target and consumed in production of X-rays. The anode materials should have high thermal conductivity, high atomic number and high melting point like tungsten, because these target materials usually get melted on high bombardment of electrons. Here Rheostat is used to regulate the intensity of x-rays by controlling the current of cathode filament [76].

3.5   X-ray Diffraction

X-ray diffraction is one of the efficient characterization method which is commonly used to find the crystalline structure of materials. X-ray diffraction gives information about crystal structure, lattice parameter, crystal alignment, particle size and defects in crystallographic structure.

This experimental technique has been long employed for analyzing crystalline structure including internal stresses and surface geometry of the crystal. It is an old characterization technique which is often used to recognize the unknown material [63]. Diffraction in a material occurs when the magnitude of inter atomic spacing matches with the wavelength of incident radiation. An X-ray of wavelength about 0.1 nm is used to get information about crystal structure [77]. When X-ray falls on the surface of material, then these rays reflected back and interfere constructively or destructively with each other depending on inter planner spacing of the material.

There is a specific phase correlation between the scattered X-rays due to regular arrangement of atoms in a crystal solid. Information about crystal structure is only obtained from constructively interfered X-rays. When phase relationship does not satisfy the condition of constructive interference, then usually destructive interference is observed in scattering directions [78].

3.5.1   Bragg's Law

Bragg's law is usually used for examining the crystalline structure and inter-planer spacing (d) of crystalline materials. Fig. 3.4 displays the schematic diagram of Bragg's law reflection. The relationship between the wavelength of the incident X-

rays, angle of incidence and inter-planer spacing is generally described by Bragg's law which is represented by equation 3.1.

$$n\lambda = 2d\sin\theta \qquad (3.1)$$

In equation 3.1, 'd' is the inter-planner spacing of a crystal, 'λ' is the wave length of X-rays and 'θ' is the scattering angle [79, 80].

Diffraction peaks of crystals are measured with the help of X-ray diffraction method, which makes it best method for examining homogeneous and inhomogeneous phases of crystalline solids. Inhomogeneous strains changes from crystal to crystal or within a single crystal, which usually result in broadening of X-ray diffraction peak having increase in scattering angle (θ) [81].
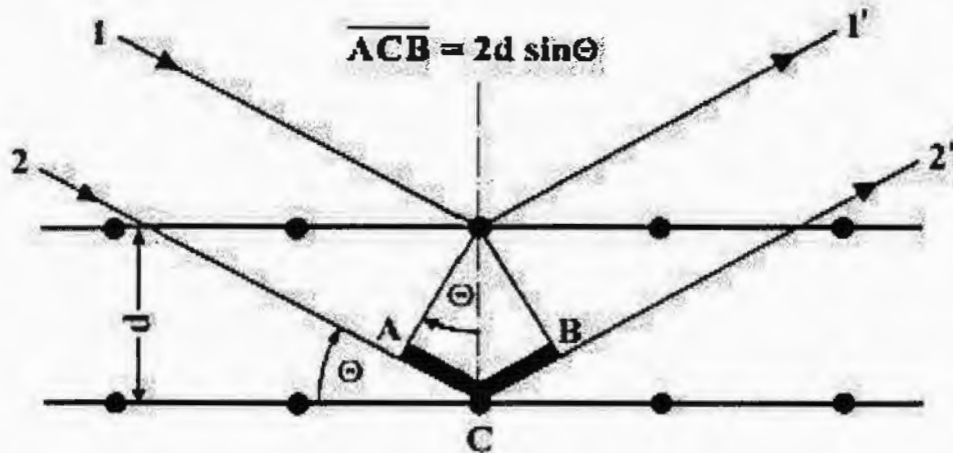
Fig. 3.4: Schematic diagram of Bragg's law reflection [78].

3.6   Diffraction Methods

For occurrence of successful diffraction, Bragg's law must be satisfied. Bragg's equation imposes tight conditions upon wavelength and angle of incidence for any type crystal. Arbitrary arrangement of crystal cannot produce diffraction, as there must be a specific arrangement of crystals to obtain the diffraction pattern by satisfying the Bragg's law. The process of diffraction can be controlled by varying experimental parameters like wavelength and angle of incidence.

31

There are three different diffraction techniques are given below,

1.   Laue method

2.   Powder method

3.   Rotating crystal method

3.6.1 Laue Method

Laue technique is used to analyze the alignment and nature of crystalline solids that is whether material is polycrystalline or single crystal. It was discovered by Laue in 1912. In this method, scattering angle is constant while wavelength varies. For analysis of crystal structure, whole range of wavelength of radiation is used. Laue camera is also used for making the photographic film. White beam of continuous spectrum is used in Laue method.
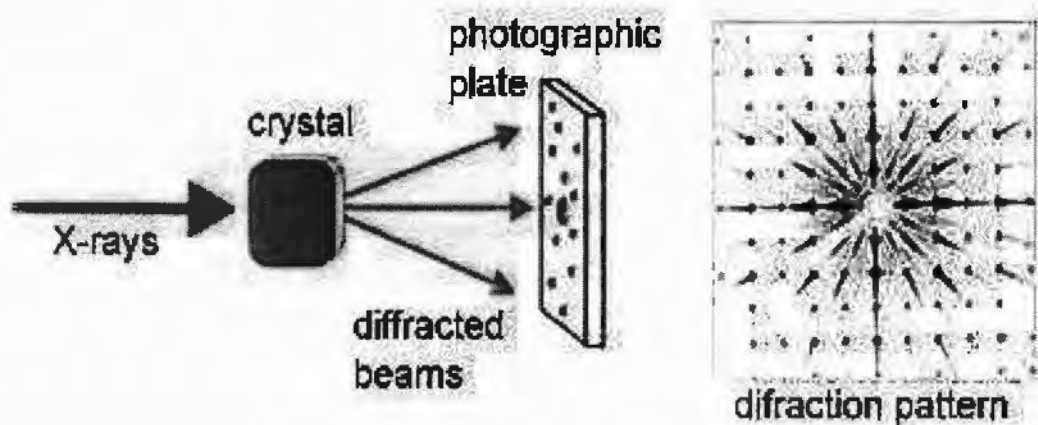
Fig. 3.5: Experimental setup of Laue method [79].

In Laue technique, crystal or sample is fixed as compared to beam of X-rays. Where all possible wavelengths are used but only those beams of X-rays give information which satisfies Brag's law. X-ray beam is diffracted and recorded on film in form of spot. This film is developed after processing it up to 5 or 6 hours. Developed film has a large number of spots and these spots are called Laue spots [82]. Experimental arrangement of Laue method is represented in Fig. 3.5.

32

3.6.2 Powder Method

In powder method, first of all crystal under analysis is converted into very fine powder and then a monochromatic beam of X-rays is allowed to fall. Every particle in the powder appears as very small crystal which is oriented in an irregular manner with respect to the incident beam of X-ray; hence there is a small chance that all the particles will be oriented in a proper way in accordance to the incident beam. In this technique, every set of crystal planes have ability to do the phenomena of reflection [78]. Fig. 3.6 shows the setup of powder method.
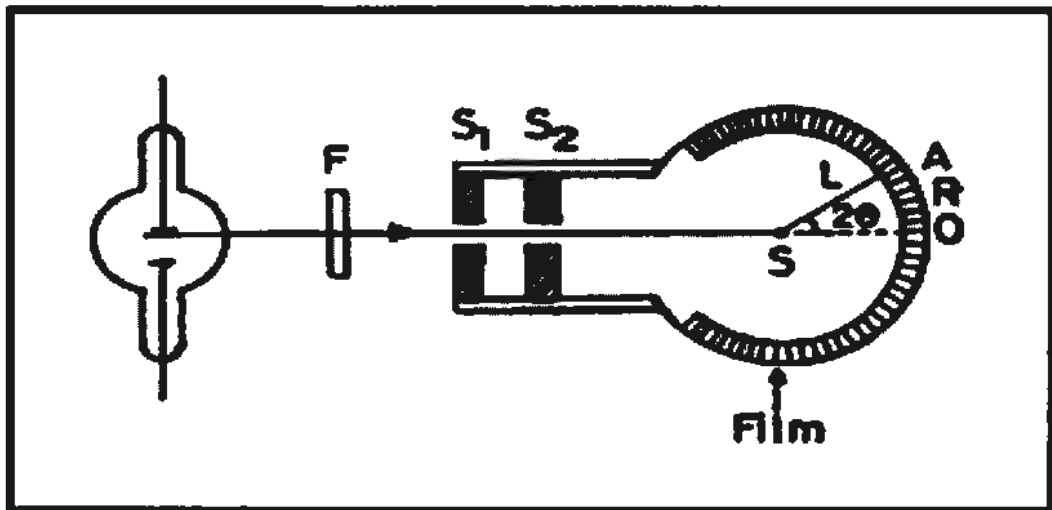
Fig. 3.6: Powder crystal spectrometer [83].

3.6.3 Rotating Crystal Method

In rotating crystal method, a crystal is adjusted along one of its axis or in some specific crystal direction which is perpendicular to the direction of monochromatic X-ray beam as demonstrated in Fig. 3.7. A thin film is adjusted around the sample crystal in cylindrical shape, where the crystal is allowed to rotate in definite direction. Both the film axis and crystal axis coincides with each other. During crystal rotation, only particular set of planes satisfy the condition of Bragg's law [78].

33
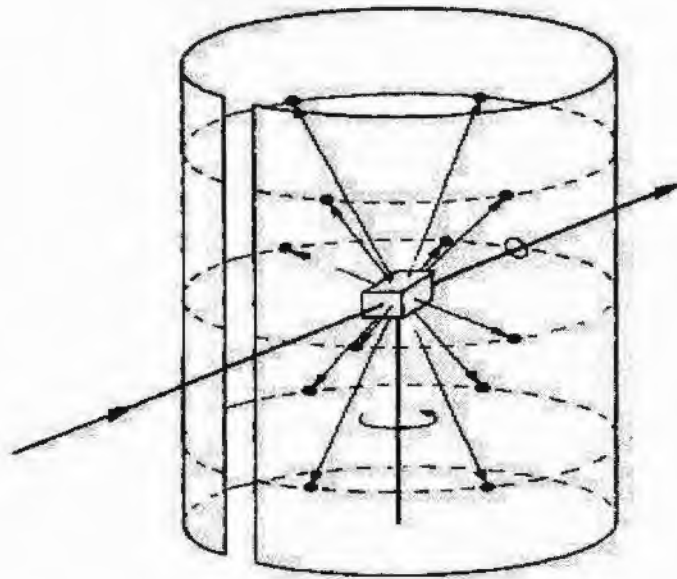
Fig. 3.7: Schematic diagram of rotating crystal technique [78].

3.7   Particle Size Determination

To find the size of particles, a famous formula known as Debye Scherrer formula is employed which is described in equation 3.2. This formula was introduced by Paul Scherrer in 1918. Its grain size measurement limitation range lies in between 0.1 and 0.2 µm.
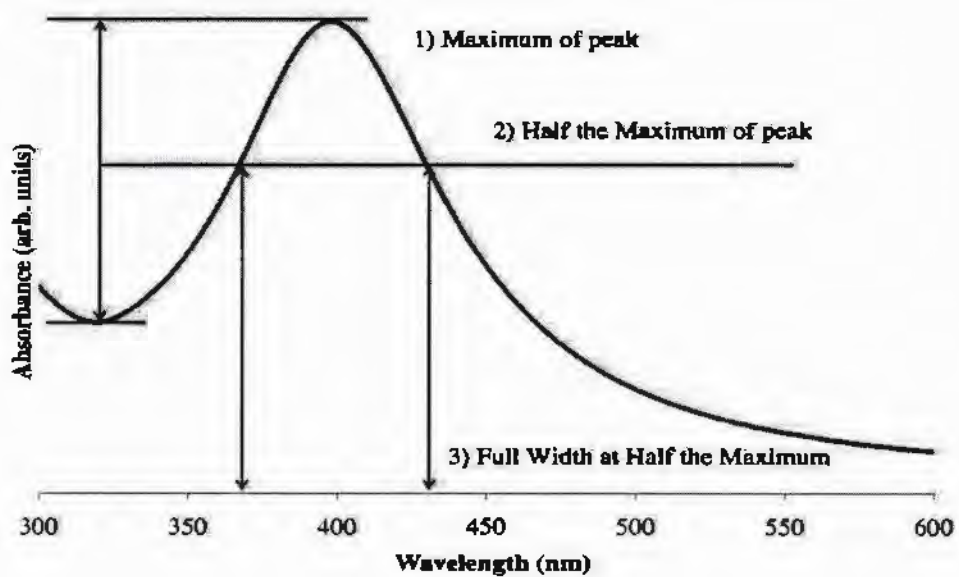
Fig. 3.8: Graph showing full width at half maximum [48].

Transmission electron microscopy is also be used to find particle size but use of Scherrer's formula is better as compared to TEM.

$$D = k\lambda / \beta cos\theta \qquad (3.2)$$

In above formula, 'B' represents the half of maximum intensity i.e. full width at half maximum and as displayed in Fig. 3.8, it is measured in units of radians. 'λ' is the wavelength of Cupper Kα-line and 'θ' shows Bragg's angle while particle width is represented by 'D'. Diffraction curve width (B) has opposite relation to the thickness of crystal like particle size reduces with the increasing width of curve [84].

3.8   Transmission Electron Microscopy (TEM)

Transmission Electron Microscopy is a method which is used to analyze the material by transmitting of electrons through the sample. There are electromagnetic lenses in TEM for the analysis of shape and size of nanoparticles. The working principle of TEM is based upon the Lorentz force, in which the magnetic field is used and focused on the lenses to get high resolution final image.

Fig. 3.9 shows the schematic diagram of TEM. The first part of TEM is "electron gun" which produces electrons at relatively higher temperature. These electrons with different accelerating voltages are passed from different lenses. Before striking the sample, the electrons are accelerated and tuned in form of a beam while passing through condenser and electromagnetic lenses. The sample which is to be analyzed is adjusted in between the two objective lenses. When beam is transmitted through the sample, a first image is formed and is shown on the fluorescent screen. There are three types of contrast are present in TEM image which are mass-thickness, phase and diffraction contrast. Mass-thickness contrast is produced by the thickness and density of the sample [85]. Therefore image is darker in those parts where sample thickness is greater. This type of issue is generally observed in larger samples.

TEM analysis uses both direct and diffracted electrons to make the image because in this way diffraction contrast increases. Diffraction contrast appears most prominently in perfect crystal structures. If there are defects and impurities in crystalline structure, then the TEM image will indicate a reduction in contrast and will show the amorphous nature of the sample. Bright or dark images are produced as a

result of phase contrast, where phase contrast is the difference between the phases of diffracted and directed electrons beams [86].
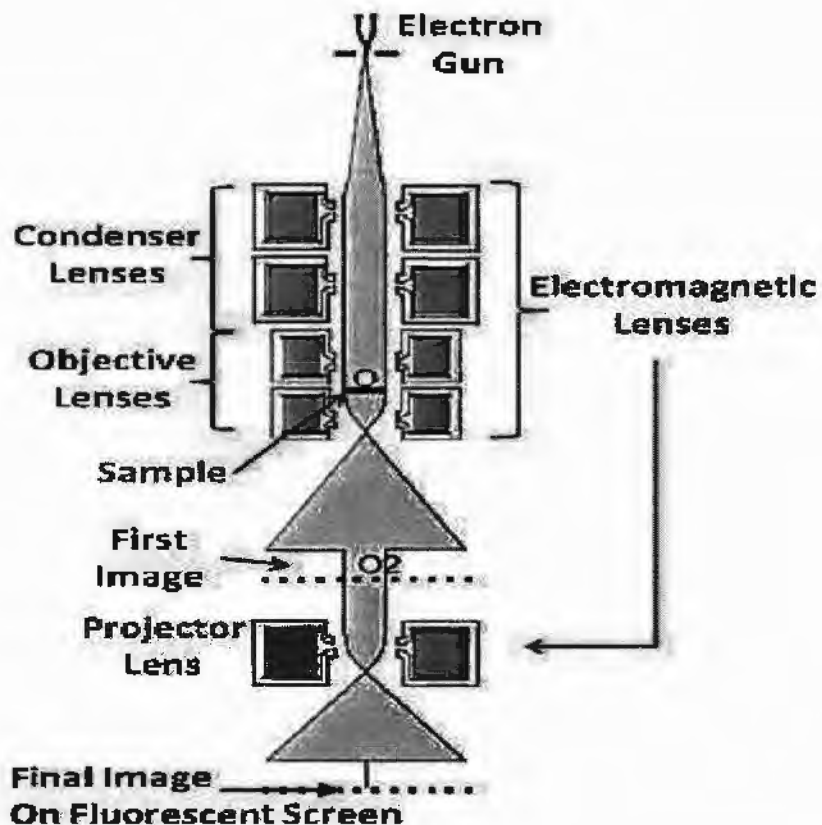
Fig. 3.9: Schematic diagram of transmission electron microscope [3].

3.9 SQUID Magnetometer

The superconducting quantum interface device (SQUID) works on the phenomena of the Josephson junction, defined by Brian Josephson in 1962. This principal was shortly derived after the microscopic theory for superconductivity which named as BCS theory (Bardeen, Cooper and Schrieffer). This theory explained the concept of fundamental particle known as Cooper pair (an electron pair with a mass of 2m and charge of 2e) [87].

A Josephson junction is composed of two semiconductors which are separated by a thin insulator and can give current flow (the electron pairs) through the tunneling barrier [88]. The generated current depends upon magnetic flux, so that is why the

36

SQUID can be used in magnetic measurement. It is also known to be very sensitive [89]. The Fig. 3.10 shows the experimental setup of SQUID magnetometer.
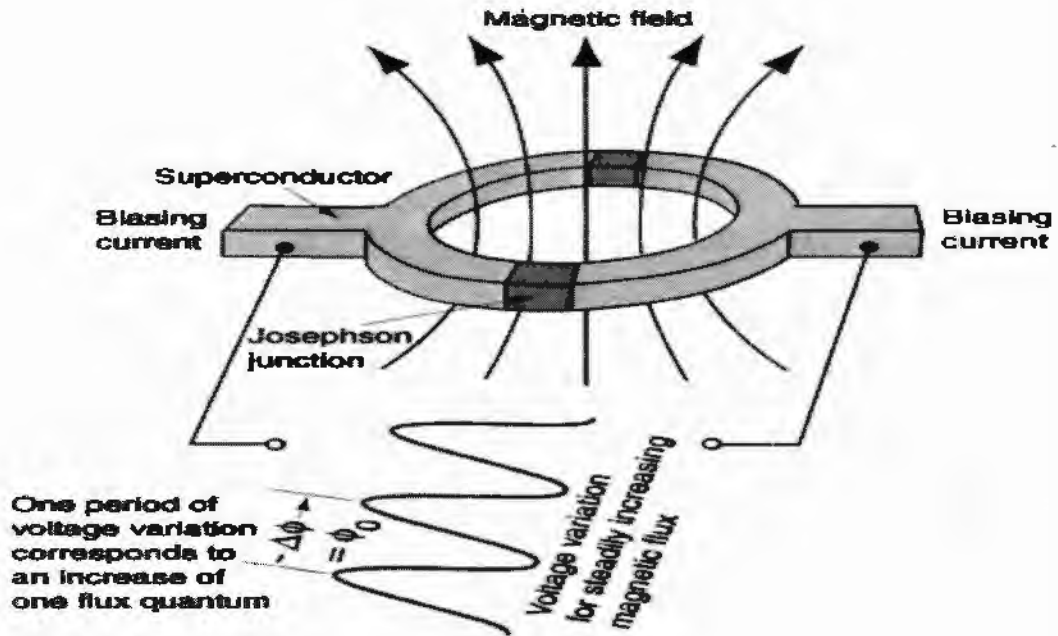
Fig. 3.10: Josephson junctions [17].

The SQUID usually operates at very low temperatures (liquid helium cooled), however there are now so-called high temperature SQUIDs emerging that can operate at temperatures around 77 K using conducting ceramics. The SQUID magnetometer is also used to measure hysteresis loops by measuring the magnetization against the applied field. By taking these measurements at different temperatures, it is possible to gather information about the saturation magnetization per unit mass and the coercivity of the material. With the help of SQUID, we can also identify the superparamagnetic nature of magnetic materials by analyzing their hysteresis loops [90-92].

37

CHAPTER 4

Results and Discussion

Spinel ferrite nanoparticles become popular in the area of research due to unique physical and chemical properties like electric, magnetic and optical properties. These unique magnetic properties include the high value of permeability, high saturation magnetization and isotropic magnetic behavior. Spinel ferrites are soft magnetic materials as they can be magnetized and demagnetized easily by applying the magnetic field, and these can also be treated as insulating materials. That is why; spinel ferrites have prominent applications in the field of biotechnology, as a catalytic agent and in preparation of magnetic materials [93].

Maghemite nanoparticles and their compounds become very popular in the field of nanotechnology in last few decades regarding to their potential use [94]. The use of maghemite nanoparticles is incredibly increased due to unique magnetic properties and non-toxic nature [45]. Iron oxide nanoparticles belong to the group of ferrites with different structural phases based on changing temperatures [95]. Maghemite nanoparticles are composed of the molecules of oxygen and hydrogen in specific proportion. Maghemite nanoparticles with diverse structural phases have varied physical properties [96, 97].

Maghemite (γ-Fe_2O_3) nanoparticles belong to the group of spinel ferrites having two lattice sites like tetrahedral and octahedral [98, 99]. Maghemite nanoparticles have ferromagnetic nature. Iron oxide nanoparticles have dynamic uses in different fields such as in catalysis, in magnetic data storage devices, in MRI, for medical diagnosing and in remote sensing [39, 100]. Magnetite and maghemite have similar chemical structure. Maghemite have also the same chemical formula $(Fe_8^{+3})_A[Fe_{40/3}^{+3}\Delta_{8/3}]_BO_{32}$ as like magnetite but with the deficiency of Fe^{+2} elements. A and B positions in the formula shows the tetrahedral and octahedral lattice sites while Δ shows the vacancy at the octahedral lattice sites [59].

Microwave plasma technique is most commonly used in the preparation of nanomaterials because it has advantage over other conventional methods, as there is high degree of excitation and ionization as compared to other formal methods of

electrical dissociation [101]. In this research, microwave plasma technique is used for the synthesis and fabrication of maghemite nanoparticles coated with non-magnetic ZrO_2. The ZrO_2 coating is used to avoid the agglomeration and to get uniformly dispersed nanoparticles [102, 103]. XRD and TEM analysis are used for structural, size and shape characterization of maghemite nanoparticles. SQUID magnetometer is used to analyze the magnetic behaviors such as AC and DC magnetic properties at different temperatures.

4.1   Structural and Phase Analysis

XRD is a well-known technique used to analyze the crystal structure and to find the average crystallite size of nanoparticles [104]. The crystal structure of the maghemite nanoparticles coated with zirconia (ZrO_2) was observed through XRD analysis. Characteristic XRD peaks of maghemite and ZrO_2 are displayed in Fig. 4.1.

Fig. 4.1 exhibits the XRD pattern of maghemite nanoparticles coated with non-magnetic ZrO_2. The indexed peaks (110), (210), (220), (311), (422) and (440) denote the miller indices of various planes of maghemite (γ-Fe_2O_3) at the diffraction angles $2\theta = 16^0$, 27^0, 31^0, 35^0, 56^0 and 61^0 respectively. The other obtained peaks (011), (002), (112) and (121) represent the miller indices of ZrO_2 at the diffraction angles $2\theta = 30°$, $35°$, $51°$ and $61°$ respectively. X-ray diffraction peaks were confirmed by comparing with standard peaks of iron oxide phases. The XRD peaks of maghemite nanoparticles were found to be matched with the pattern of the inverse spinel structure of maghemite. The most intense peaks are (011) and (311) which belong to the coated material ZrO_2 and maghemite respectively. XRD peaks from other crystal structure were not detected, which shows that ZrO_2 coated maghemite nanoparticles had high purity and crystallinity. The huge peaks correspond to Al substrate.

Average particle size of maghemite nanoparticles is measured by using Debye Scherrer's formula,

$$D = k\lambda / \beta cos\theta \qquad (4.1)$$

In equation (4.1), 'D' is grain size, 'K' is constant with value equal to 0.91, 'λ' is the wavelength of X-ray radiation, 'θ' is diffraction angle and 'β' is the line width

at half maximum height. Average crystallite size of maghemite comes out to be 14 nm while crystallite size of coating material (ZrO_2) is about 5 nm as calculated by Debye-Scherrer's formula [105, 106].
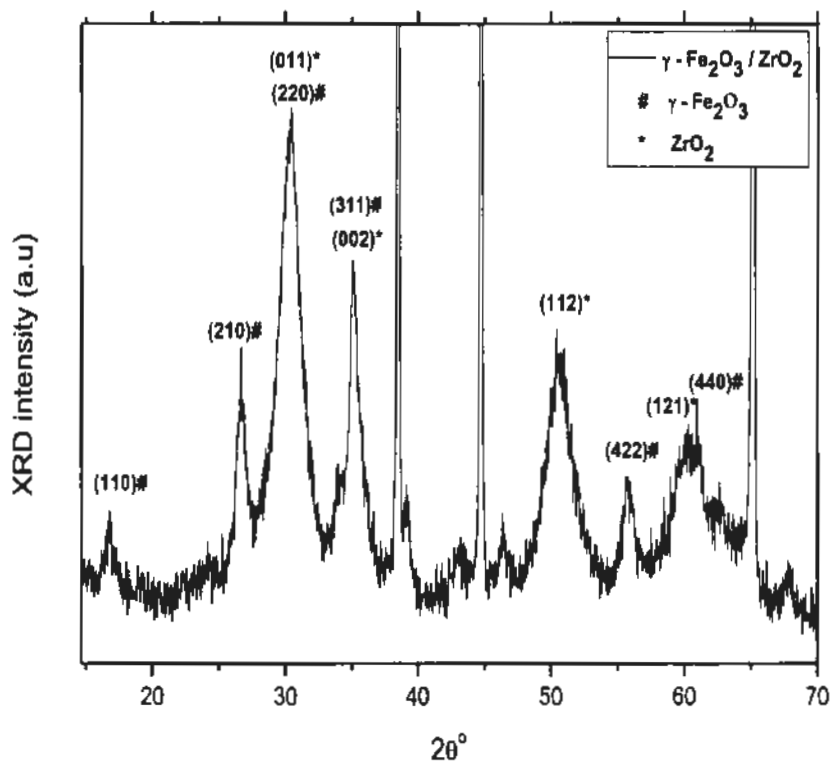
Fig. 4.1: XRD peaks of ZrO_2 coated maghemite nanoparticles.

4.2   Transmission Electron Microscopy

Transmission electron microscopy is used to study the size, shape and morphology of particles. Fig. 4.2 indicates the TEM image of ZrO_2 coated maghemite nanoparticles at the magnification scale of 50 nm. It is clear from the figure that the nanoparticles are well dispersed and small in size. The TEM image also reveals that the nanoparticles are highly crystalline and non-agglomerated. The shape of maghemite nanoparticles is almost spherical with narrow size distribution [107, 108]. It is clear from the Fig. 4.2 that most of the nanoparticles are non-agglomerated due to presence of ZrO_2 coating. The ZrO_2 coating acts as a spacer between nanoparticles which avoids the agglomeration of nanoparticles.

40
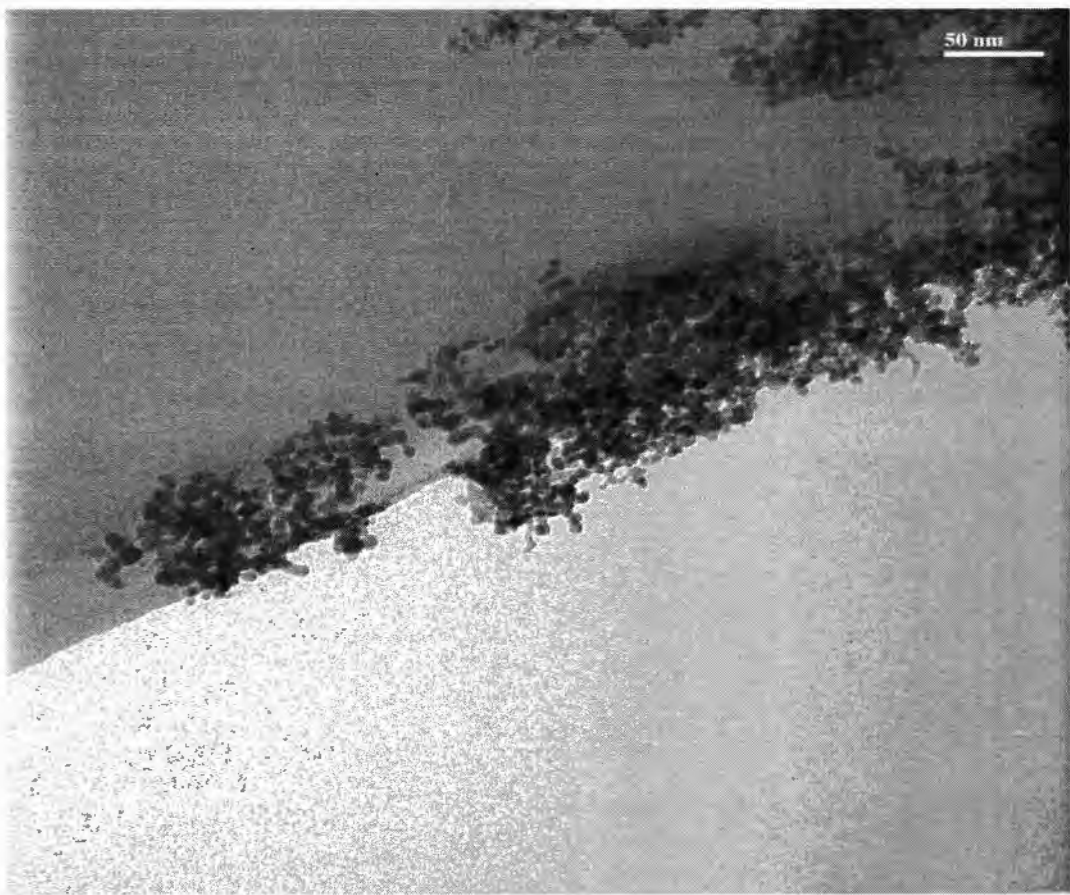
Fig. 4.2: TEM image of ZrO$_2$ coated maghemite nanoparticles at 50 nm scale.

4.3 Magnetic Properties

The AC and DC magnetic properties of ZrO$_2$ coated maghemite nanoparticles were studied and analyzed by using SQUID magnetometer, which is very sensitive characterization instrument and usually used to find the magnetic field of low strength with small value of tesla and resolution up to 10^{-11} G. It is helpful in the analysis of properties of magnetic nanoparticles over different series of temperatures and magnetic field strengths [109]. In this research, there is focus upon the hysteresis loops, blocking temperatures, anisotropy effect and spin-flip time. The temperature dependent M-H hysteresis loops, M-H loop at fixed temperature (5K) and field cooled/zero field cooled (FC-ZFC) curves are also being characterized with the help of SQUID magnetometer.

4.3.1 Zero Field and Field Cooled Magnetization Curves

The temperature dependence of zero field cooled and field cooled magnetization is measured by applying field of 50 Oe and it is shown in the Fig. 4.3.

41

The system is first cooled from 300 K to 4.2 K in a zero applied field to obtain the ZFC magnetization curve. Furthermore, magnetic field is applied with regular increase of temperature and consequently the FC magnetization curve is drawn [110, 111]. Moreover, the ZFC curve overlaps with the curve of the FC at higher temperatures and separates from the ZFC at junction temperature Tj = 220 K [112].
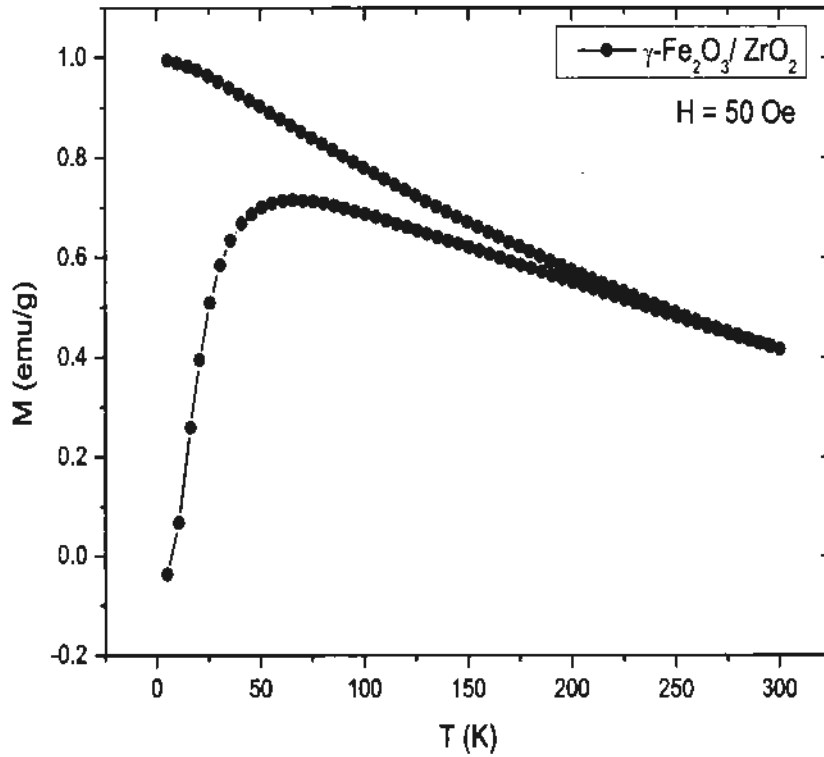
Fig. 4.3: FC-ZFC curve of maghemite nanoparticles coated with ZrO_2.

The ZFC curve shows maximum around 65 K. These magnetic nanoparticles become thermally unstable (above blocking temperature) showing the superparamagnetic property. The magnetization of nanoparticles exponentially reduces as KV/k_BT. These magnetic nanoparticles represent distinctive strong magnetic fields at relatively low temperatures but this property reduces as the temperature is increased. When nanoparticles are chemically coated with non-magnetic materials, then their blocking temperature reduces to lower temperature values. The surface energy of the nanoparticles is increased when there is no coating of any surfactant material. As a result, there is strong interparticle interaction and agglomeration of nanoparticles.

These agglomerated nanoparticles link with each other in form of clusters, which results in an increase of the blocking temperature. therefore, ZrO_2 coated maghemite nanoparticles are more easily aligned with the external magnetic field as compared to bare maghemite nanoparticles [112]. The net magnetization of surface coated maghemite nanoparticles is found to be reduced, which is attributed to non-collinear surface spin arrangement.

4.3.2 M-H Hysteresis Loop at 5K Temperature

Magnetic hysteresis loop of maghemite nanoparticles coated with non-magnetic ZrO_2 is drawn with the help of SQUID magnetometer at 5K temperature by applying ±5 T magnetic field and it is shown in Fig. 4.4. The M-H hysteresis loop shows the ferrite nature of magnetic maghemite nanoparticles. The inset figure shows the clear hysteresis loop with coercivity (H_c) value of 184 Oe. Frozen surface spins are stacked on the surface of nanoparticles and have strong interactions with core shell spins. The H_c is largely increased by this property of spins at low temperatures [113].
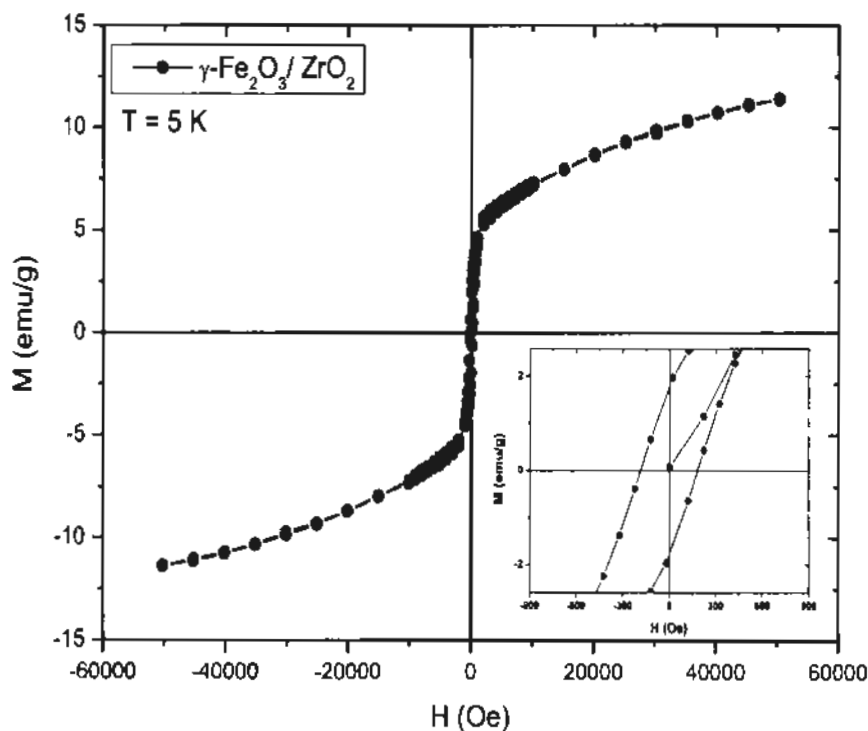
Fig. 4.4: M-H loop at 5 K temperature with an inset graph of coercivity.

43

In the presence of strong magnetic field, the spins of individual nanoparticles start aligning in the direction of field and reaches maximum saturation magnetization (M_s) value. The measured value of M_s is 11.4 emu/g. This value of M_s is less than the corresponding bulk M_s value (M_s = 80 emu/g) which is characteristic for maghemite nanoparticles due to non-collinear spin structure of surface spins. There is enhancement in M_s value at low temperatures (5 K) and it is due to the reduced spin vibrations at nanoparticles surface [114, 115].

H_c is also significant parameter of hysteresis loop that can be affected by dipolar and exchange interactions. Kodama *et al.* [47] also presented a computational model of magnetic behavior showing disordered spin freezing on surface of ferrite nanoparticles. Where the existence of smaller M_s for ferrite nanoparticles is attributed to the randomly arranged surface spins. Verdes *et al.* [90] showed a mathematical model about the enhancement of H_c with increasing agglomeration of particles.

4.3.3 Temperature Dependent M-H Partial Loops

The magnetization measurements were done by using SQUID magnetometer at maximum applied field up to ±5 T with varying temperatures. Fig. 4.5 represents the schematic diagram of M-H partial hysteresis loops at different temperatures 5, 25, 50, 75, 100, 150 and 250 K for the applied magnetic field of ±5 T. The H_c values are 184, 26.6, 5.9, 2, 0, 0 and 0 Oe at their respective temperatures of 5, 25, 50, 75, 100, 150 and 250 K respectively. There is typical growth in coercivity values of nanoparticles with diminishing temperatures. The basic reason behind the increasing Hc with reducing temperatures is the spin glass behavior and pinning of surface spins. The other cause of huge value of H_c at lower temperatures is the core shell interaction of nanoparticles [116]. M_s values are calculated to be 11.4, 7.5, 6.6, 6.3, 6, 5.7 and 5.3 emu/g at their respective temperatures of 5, 25, 50, 75, 100, 150 and 250 K respectively.

One of the significant property of the M-H partial hysteresis loops is that at lower temperatures, the magnetic moments of the nanoparticles do not completely saturate even by applying high magnetic field of 50 kOe and this is usually due to the random and non-collinear surface spins of the nanoparticles. Size dependent decrease in M_s is distinctive property of ferrite nanoparticles which is attributed to disordered surface spins [117].

44
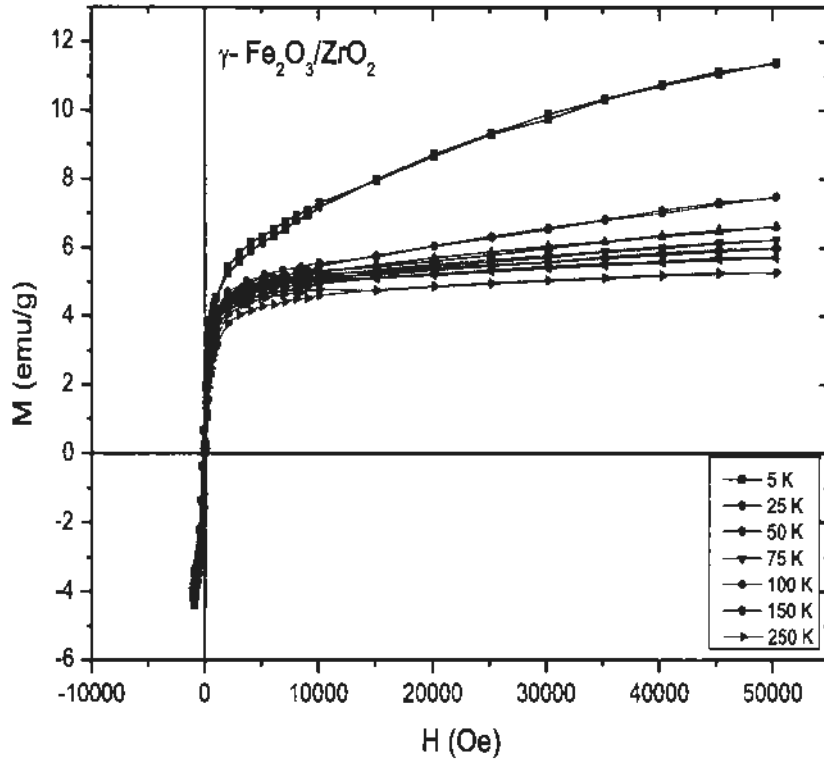
Fig. 4.5: M-H partial loops of maghemite nanoparticles at different temperatures.

4.3.4 Saturation Magnetization and Bloch's Law Fitting

The M_s values plotted against varying temperatures ranging from 5 to 250 K are shown in Fig. 4.6. For very large ferromagnetic arrangement, M_s below the Curie temperature (Tc) follows the Bloch's law [118].

$$M_s(T) = M_s(0) \ (1 - BT^b) \qquad (4.2)$$

In equation 4.2, '$M_s(T)$' is the temperature dependent saturation magnetization, '$M_s(0)$' is the spontaneous magnetization at zero kelvin, 'B' is the Bloch's constant (fitting parameter) which is dependent upon material structure and 'b' is the Bloch's exponent (fitting parameter). Bloch's law is usually effective for ferromagnetic and ferrimagnetic bulk materials including ferrites [118, 119]. According to Bloch's law, the temperature dependent magnetization is due to the excitation of spin waves [120].

45

In the Fig. 4.6, the M_s value (11.4 emu/g) corresponding to T= 5 K is very large and it exceeds the range of Bloch's law fit, so in this fitting, we only use the remaining M_s values without considering M_s=11.4 emu/g. In this fitting, M_s shows the usual increase with reducing temperature which is due to the existence of freezed and canted surface spins. Furthermore the fitting was not converging at lower temperatures because of the reducing M_s values. In ZrO_2 coated maghemite nanoparticles, the alignment of surface magnetic moments and their exchange interactions with the core shell magnetic moments is usually changed because of interaction with surface coating material. The ZrO_2 coating of these nanoparticles eases the alignment of core shell spins with external magnetic field and that is the reason due to which M_s is improved at lower temperatures [49].
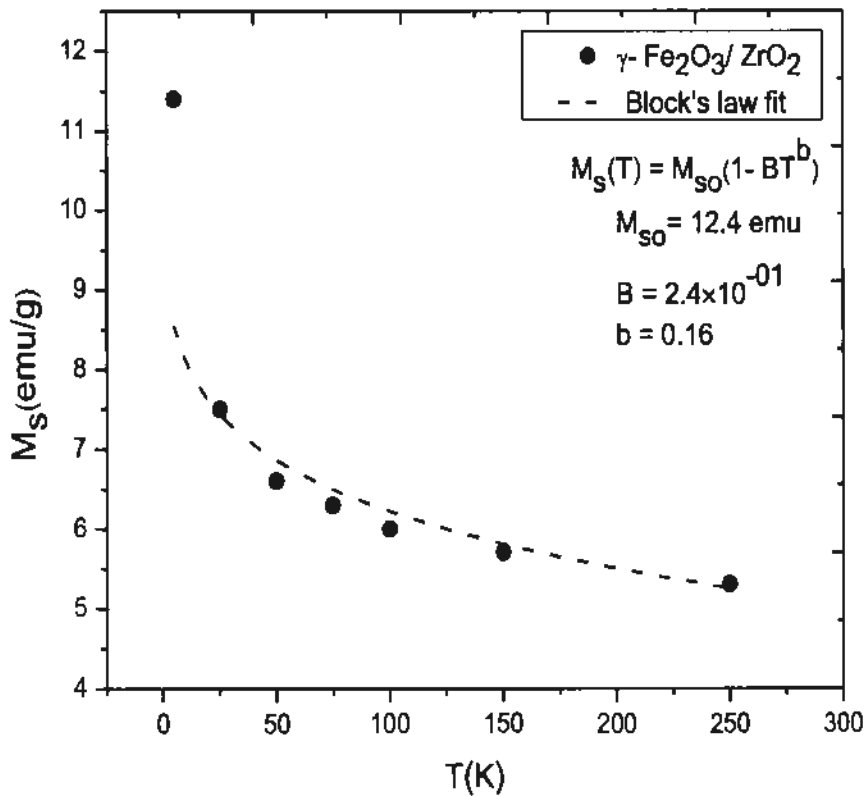
Fig. 4.6: Bloch's law fitting for ZrO_2 coated maghemite nanoparticles.

The value of Bloch's exponent is b = 0.16 for a 3D arrangement. Fitting of Bloch's law produces: $B = 2.4 \times 10^{-01}$ and $M_s(0) = 12.4$ emu/g by using equation 4.2.

46

Bloch's law represents normal fitting for non-magnetic ZrO_2 coated maghemite nanoparticles.

4.3.5 Coercivity

The temperature dependence of H_c for uniformly dispersed single domain magnetic nanoparticles with one dimensional anisotropy can be explained in the form of a mathematical model known as Kneller's law [115]. The plot of H_c vs. T with nonlinear graph follows the Kneller's law.

$$H_c = H_c(0) \left(1 - (T/T_B)^{1/2}\right) \qquad (4.3)$$

In equation 4.3, '$H_c(0)$' is the coercivity at 0 K and 'T_B' is the average blocking temperature. We tried to fit the Kneller's law but it did not converge at low temperatures due to frozen surface spin effects.
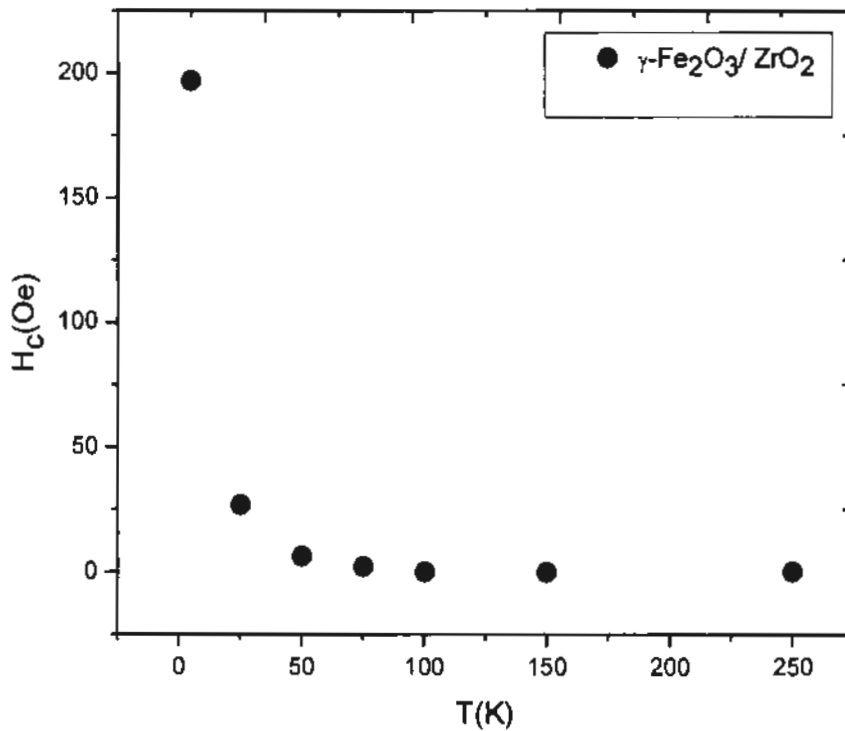
Fig. 4.7: Temperature dependence of Hc of ZrO_2 coated maghemite nanoparticles.

Fig. 4.7 shows the temperature dependence of H_c of ZrO_2 coated maghemite nanoparticles. The nanoparticles usually have large H_c values at low temperatures

47

because of their strong surface anisotropy. The coercivity value in this specific situation is affected by many factors rising mainly from different particle size distribution [121, 122]. There will be large deviation from Kneller's law if the volume of the single domain particles differs in a broader range [123, 124].

4.4   Frequency Dependent AC Susceptibility

Frequency dependent AC susceptibility measurements gives us information about the measuring time and magnetic state of blocked nanoparticles which are determined by the anisotropy energy barrier ($E_a = K_{eff}V$). Temperature dependent AC susceptibility is also used to measure the change in T_B with shift in frequency. Fig. 4.8 represents the frequency dependence of in-phase AC susceptibility of ZrO_2 coated maghemite nanoparticles in frequency range from 0.1 to 1000 Hz.
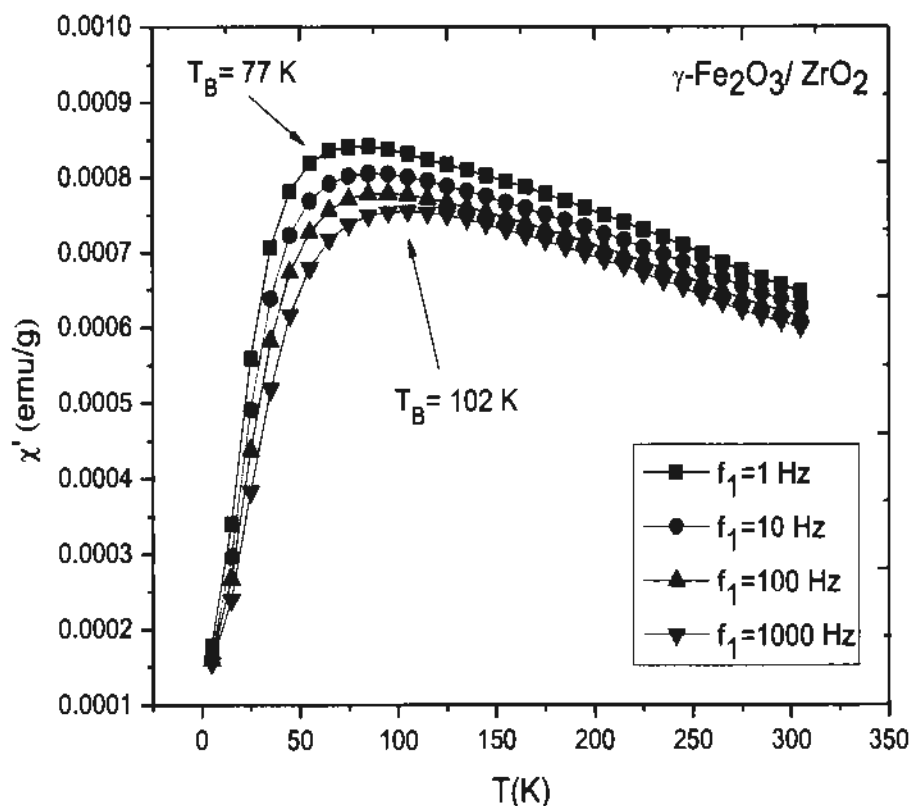
Fig. 4.8: In-phase AC susceptibility of ZrO_2 coated maghemite nanoparticles.

Here first nanoparticles are cooled from room temperature to 4.2 K in the absence of external magnetic field and then AC susceptibility is measured with an

increasing temperature. The T_B is increased from 77 K to 102 K as the frequency is shifted from 1 to 1000 Hz. The smaller change in T_B with increasing frequency is due to enhanced interparticle interactions. Dipolar and exchange interactions are also operative in maghemite nanoparticles, which make the system stiffer causing smaller change in T_B with an increasing frequency.

AC frequency dependent magnetization includes the different types of fitting laws like Arrhenius law, Vogel-Fulcher law and Dynamic scaling law. All fitting graphs of these laws are dependent upon T_B and measuring time (τ). AC frequency dependent magnetization is not only used to investigate the magnetic state of nanomaterials but also gives information about the dynamics of the nanoparticles system. These laws are used to get the information about the atomic spin flip time, dispersed nature and spin glass behavior of nanoparticles.

4.4.1 Arrhenius Law Fitting

The dynamics of magnetic relaxation were studied with the help of AC magnetic susceptometry. Arrhenius law is used for measuring the time of mono-dispersed and non-interacting single domain blocked particles with uniaxial anisotropy barrier energy (E_a) [125].

$$\tau = \tau_0 exp\ (E_a/k_B T_B) \tag{4.4}$$

Where 'τ' is the measuring time of the spin flip of a nanoparticle, 'τ_0' is the atomic spin flip time required for magnetic vector (dependent upon gyro-magnetic ratio, particle volume and damping constant), 'E_a' is the anisotropy energy, $K_B T_B$ is the thermal energy. The average anisotropy barrier is $E_a = K_{eff}\ V$, where 'K_{eff}' is the effective anisotropy energy constant and 'V' is the average volume of particle. The value of E_a and frequency can be readily attained by AC magnetic susceptometry measurements [126]. When there is large enough separation between the nanoparticles, then interparticle interactions between magnetic moments are insignificant. The Fig. 4.9 shows the Arrhenius law fitting of maghemite nanoparticles with graph plot of time (t) vs. blocking temperature ($1/T_B$).
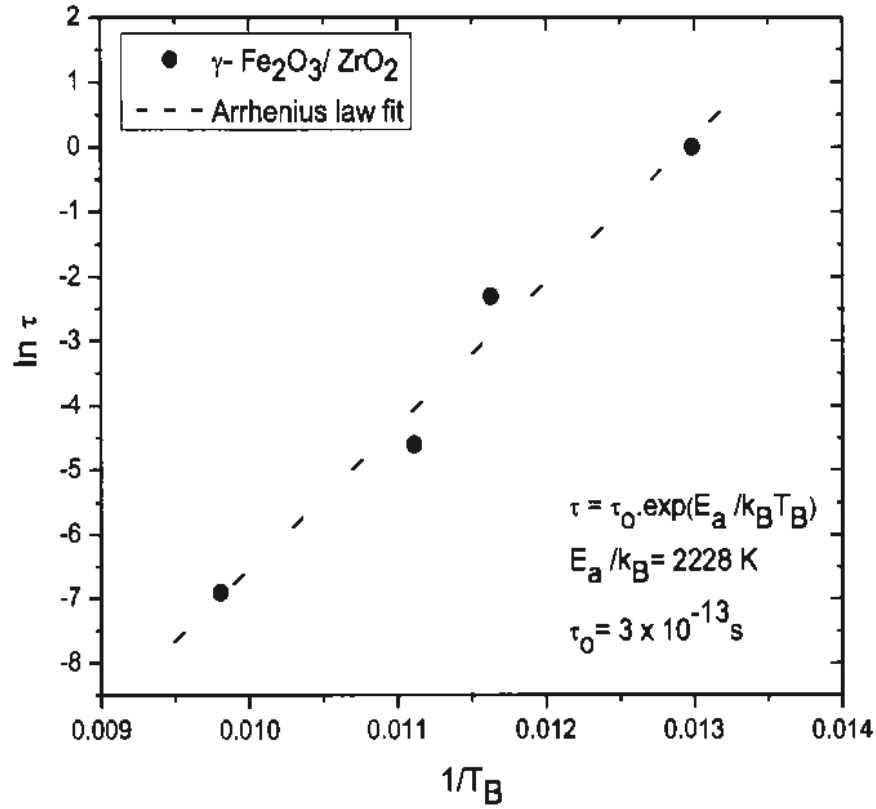
Fig. 4.9: Arrhenius law fit for ZrO_2 coated maghemite nanoparticles.

Owing to superparamagnetic behavior near the blocking temperature, where the measuring time of the spin flip becomes equal to zero, the anisotropy energy becomes very small as compared to thermal energy and the direction of the spin flip changes quickly giving rise to thermal oscillation between magnetic nanoparticles [49].

The above graph shows the straight line with fitting parameter of activation energy E_a/k_B is equal to 2228 K and atomic spin flip time $\tau_0 = 3 \times 10^{-13}$ s. The value of τ_0 does not lie in the range of standard value (10^{-9} to 10^{-12} s), also E_a/k_B gives unphysical value which exceeds the standard value calculated for ferrimagnetic materials. Both fitting parameter values given by Arrhenius law are not reasonable, so our particles system don't follow the Arrhenius law. Now some other laws are employed for measurement of reasonable values of E_a/k_B and τ_0.

4.4.2 Vogel-Fulcher Law Fitting

The two parameters τ_0 and E_a/k_B of Arrhenius law fit are inadequate, so there is need of an improved analysis using the Vogel-Fulcher law [110]. The Vogel-Fulcher law is described in Eq. 4.5 with an extra parameter T_0, showing the strength of interparticle interactions,

$$\tau = \tau_0 exp\ (E_a/k_B\ (T\text{-}T_0))\qquad\qquad(4.5)$$

In equation 4.5, 'τ' is the relaxation time of spin flip of nanoparticles, 'τ_0' is the atomic spin flip time, 'E_a' is the anisotropy energy barrier, '$k_B T$' is the thermal activation energy and 'T_0' is the fitting interaction parameter.
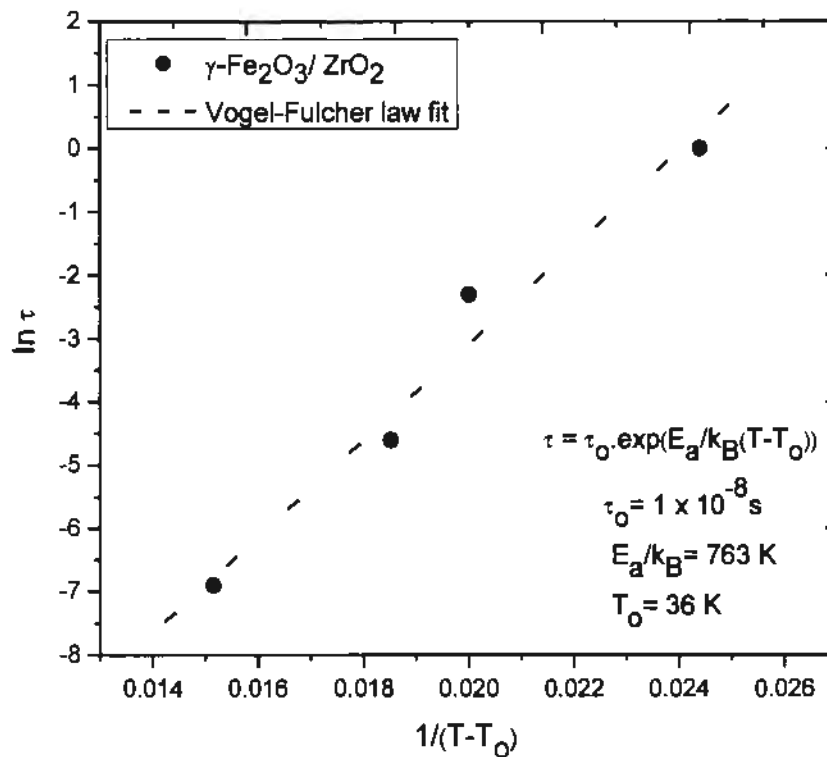
Fig. 4.10: Vogel-Fulcher law fit for maghemite nanoparticles coated with ZrO_2.

Fig. 4.10 displays the outcomes the Vogel-Fulcher law fitting. The value of $\tau_0 = 1 \times 10^{-8}$ s, activation energy parameter $E_a/k_B = 763$ K and T_0 value from the best fit is 36 K. The τ_0 and E_a/k_B uses reasonable values for ZrO_2 coated maghemite nanoparticles. The value of T_0 shows that maghemite nanoparticles have interparticle interactions. The graph of Fig. 4.10 is totally linear which shows that relaxation time

is directly proportional to the inverse of temperature. Moreover τ_0 and E_a/k_B values are comparable to the standard values measured for ferrimagnetic and ferromagnetic nanoparticles, which shows that these nanoparticles are interacting.

4.4.3 Dynamic Scaling Law Fitting

After using the Vogel-Fulcher law for ZrO_2 coated maghemite nanoparticles, now we will check the possibility of spin glass property in maghemite nanoparticles by using Dynamic scaling law fit. There are mainly two types of spin glass states in nanoparticles, first one is the super spin glass state and second one is the surface spin glass state.

Nanoparticles with or without non-magnetic medium may become frozen at lower temperatures which is attributed to particles magnetic dipolar interactions and identified as super spin glass state. Dynamic scaling law is generally used to analyze spin glass systems. The following time scaling law is used for critical dynamics systems [127].

$$\tau = \tau^* \left[T_0/(T_S - T_0) \right]^{zv} \tag{4.7}$$

In equation 4.7, 'τ' is the experimental measuring time of freezed surface spins, 'τ^*' is related to the coherence time of joined distinct atomic magnetic moments, 'T_0' is the "fixed" spin glass transition temperature, "zv" is the critical exponent ranging from 4 to 12 for different spin glass freezing systems [115, 128] and 'T_S' is the frequency dependent freezing temperature. Dynamic scaling law shows that there is a critical decrease in relaxation time close to the spin glass transition temperature. Fig. 4.11 represents the results of Dynamic scaling law fitting for maghemite nanoparticles coated with ZrO_2. It gives the result of transition temperature $T_0 = 70$ K which is in good agreement with the T_B of the FC-ZFC curve (see Fig. 4.3).

Fitting of Dynamic scaling law gives us reasonable results of $\tau^* = 6 \times 10^{-5}$ s and $zv = 5.75$. The enhanced value of τ^* is attributed to frozen and randomly arranged surface spins, therefore have much greater relaxation time as a compared to single atomic spins. The value of critical exponent falls in the range of spin glass regime which specifies the presence of spin glass effect in maghemite nanoparticles [129].
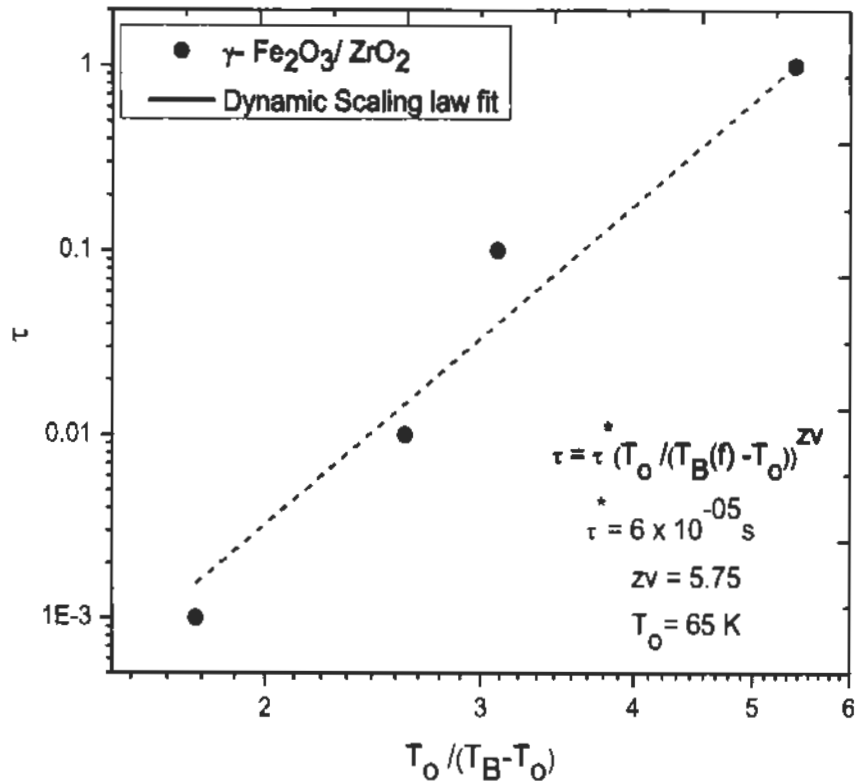
Fig. 4.11: Fitting of scaling law to the frequency dependent AC-susceptibility of maghemite nanoparticles.

Table 4.1: Values of fitted parameters from Arrhenius law, Vogel-Fulcher law and Dynamic scaling law fits.

Law	Parameter	Values
Arrhenius law	τ_O	3×10^{-13} s
	E_a/k_B (K)	2228 K
Vogel-Fulcher law	τ_O	1×10^{-8} s
	E_a/k_B (K)	763 K
	T_O (K)	36 K
Dynamic scaling law	τ^*	6×10^{-5} s
	zv	5.75
	T_O (K)	65 K

4.5   Conclusion

We have studied the AC and DC magnetic properties of maghemite (γ-Fe$_2$O$_3$) nanoparticles coated with zirconia (ZrO$_2$) prepared by microwave plasma synthesis. This synthesis method avoids interparticle interaction of nanoparticles due to charging in the plasma. ZrO$_2$ coating has significant effects on the structural, AC and DC magnetic properties of maghemite nanoparticles. The structural and phase configuration of nanoparticles were characterized using the X-ray diffraction method which confirms inverse spinel structure for maghemite nanoparticles. The blocking temperature (T_B) of temperature dependent zero field cooled/field cooled (ZFC-FC) takes value 65 K at an applied field of 50 Oe. Temperature dependent M-H hysteresis loop at 5 K indicates the small value of saturation magnetization (M_s) 11.4 emu/g as compared to bulk saturation magnetization value (80 emu/g) and it is accredited to non collinear surface spins. The typical growth in coercivity with reducing temperatures of M-H loops is attributed to random and frustrated spins at the surface. Bloch's law shows normal fitting for non-magnetic ZrO$_2$ coated maghemite nanoparticles in temperature range from 5 K to 250 K having increasing trend of saturation magnetization with decreasing temperatures and this property is due to the exchange interactions of surface spins with the core shell magnetic moments. Arrhenius law does not fit to AC frequency dependent magnetization data. Such an attempt results in unphysical values of atomic spin flip time τ_0 (3×10^{-13}s) and activation energy E_a/k_B (2228 K). Fit to the Vogel-Fulcher law relax the unreasonable results of fitting parameters and provides reasonable value for atomic spin flip time (1×10^{-8}s). Dynamic scaling law fit supports the presence of spin glass behavior. It yields proper value of critical exponent "zv" (5.75) in the range of spin glass state. Randomly freezed frustrated surface spins of maghemite nanoparticles are responsible for surface spin glass effect. The main origin of enhanced surface effects in ZrO$_2$ coated nanoparticles. is primarily frustrated spins at the surface. All measurements specify the existence of moderate interparticle (dipolar) interactions among nanoparticles. In conclusion, ZrO$_2$ surface coating can be beneficial to control the nanoparticle size and to tailor the structural as well as magnetic properties of the maghemite nanoparticles for diverse applications.

References

[1]   E. Roduner, "Size matters: why nanomaterials are different," *Chemical Society Reviews,* vol. 35, no. 7, pp. 583-592, 2006.

[2]   R. Aitken, M. Chaudhry, A. Boxall *et al.,* "Manufacture and use of nanomaterials: current status in the UK and global trends," *Occupational medicine,* vol. 56, no. 5, pp. 300-306, 2006.

[3]   C. W. Shong, C. H. Sow, and A. T. Wee, *Science at the nanoscale: an introductory textbook*: Pan Stanford Publishing, 2010.

[4]   S. Horikoshi, and N. Serpone, *Microwaves in nanoparticle synthesis: fundamentals and applications*: John Wiley & Sons, 2013.

[5]   A. I. Gusev, and A. A. Rempel', *Nanocrystalline materials*: Cambridge Int Science Publishing, 2004.

[6]   A. Gadkari, T. Shinde, and P. Vasambekar, "Structural and magnetic properties of nanocrystalline Mg–Cd ferrites prepared by oxalate co-precipitation method," *Journal of Materials Science: Materials in Electronics,* vol. 21, no. 1, pp. 96-103, 2010.

[7]   Y. Huang, D. Hunston, A. Kinloch *et al.,* "Toughened plastics I," *Advances in chemistry series,* vol. 233, pp. 1-38, 1993.

[8]   S. Chikazumi, *Physics of Magnetism,* p.^pp. 281–391, New York: Wiley, 1964.

[9]   S. Ayyappan, S. Mahadevan, P. Chandramohan *et al.,* "Influence of Co2+ ion concentration on the size, magnetic properties, and purity of CoFe2O4 spinel ferrite nanoparticles," *The Journal of Physical Chemistry C,* vol. 114, no. 14, pp. 6334-6341, 2010.

[10] K. Widder, G. Flouret, and A. Senyei, "Magnetic microspheres: synthesis of a novel parenteral drug carrier," *Journal of Pharmaceutical Sciences,* vol. 68, no. 1, pp. 79-82, 1979.

[11] P. Gupta, C. Hung, F. Lam *et al.,* "Albumin microspheres. III. Synthesis and characterization of microspheres containing adriamycin and magnetite," *International journal of pharmaceutics,* vol. 43, no. 1, pp. 167-177, 1988.

[12] J. A. Sargent, and F. A. Gotch, "Principles and biophysics of dialysis," *Replacement of renal function by dialysis,* pp. 34-102: Springer, 1996.

[13] S. Blundell, *Magnetism in condensed matter*: Oxford Univ. Press, 2001.

[14] D. L. Leslie-Pelecky, and R. D. Rieke, "Magnetic properties of nanostructured materials," *Chemistry of materials,* vol. 8, no. 8, pp. 1770-1783, 1996.

[15] K. Yasugi, Y. Nagasaki, M. Kato *et al.,* "Preparation and characterization of polymer micelles from poly (ethylene glycol)-poly (D, L-lactide) block copolymers as potential drug carrier," *Journal of controlled release,* vol. 62, no. 1, pp. 89-100, 1999.

[16] C. Kittel, *Introduction to solid state physics*: Wiley, 2005.

[17] K. H. J. Buschow, and F. R. Boer, *Physics of magnetism and magnetic materials*: Springer, 2003.

[18] B. Bleaney, and K. Bowers, "Anomalous paramagnetism of copper acetate." pp. 451-465.

[19] B. Veriansyah, J.-D. Kim, B. K. Min *et al.,* "Continuous synthesis of magnetite nanoparticles in supercritical methanol," *Materials Letters,* vol. 64, no. 20, pp. 2197-2200, 2010.

[20] P. Atkins, *Shriver and Atkins' inorganic chemistry*: Oxford University Press, USA, 2010.

[21]   C. Sorensen, "Magnetism," *Nanoscale materials in chemistry*, pp. 169-221, 2001.

[22]   D. S. Mathew, and R.-S. Juang, "An overview of the structure and magnetism of spinel ferrite nanoparticles and their synthesis in microemulsions," *Chemical Engineering Journal*, vol. 129, no. 1, pp. 51-65, 2007.

[23]   R. Silberglitt, J. Schwarz, C. Contescu *et al.*, "Dekker Encyclopedia of Nanoscience and Nanotechnology," Taylor & Francis, 2004.

[24]   J. S. Smart, "The Néel theory of ferrimagnetism," *American Journal of Physics*, vol. 23, no. 6, pp. 356-370, 1955.

[25]   D. K. Cheng, *Field and Wave Electrodynamics*, 2nd edition ed.: Addison Wesley Publishing Company 1983.

[26]   T. Tanaka, "Effects of the Oxygen Nonstoichiometry on the Domain Structure and the Initial Permeability in Mn–Zn Ferrites," *Japanese Journal of Applied Physics*, vol. 17, no. 2, pp. 349, 1978.

[27]   M. Vucinic-Vasic, M. Boskovic, A. Antic *et al.*, "Temperature induced evolution of structure/microstructure parameters and their correlations with electric/magnetic properties of nanocrystalline Nickel ferrite," *Ceramics International*, vol. 40, no. 3, pp. 4521-4527, 2014.

[28]   C.-L. Chen, and C.-L. Dong, "Characterization of the Electronic Structure of Spinel Superconductor LiTi2O4 using Synchrotron X-ray Spectroscopy," *SUPERCONDUCTORS–NEW DEVELOPMENTS*, pp. 17, 2015.

[29]   S. Son, M. Taheri, E. Carpenter *et al.*, "Synthesis of ferrite and nickel ferrite nanoparticles using radio-frequency thermal plasma torch," *Journal of Applied Physics*, vol. 91, no. 10, pp. 7589-7591, 2002.

[30]   A. J. Decker, *Solid State Physics*: Mc Milan Press Ltd. London 1995.

[31]   T. Nakamura, T. Miyamoto, and Y. Yamada, "Complex permeability spectra of polycrystalline Li–Zn ferrite and application to EM-wave absorber," *Journal of magnetism and magnetic materials*, vol. 256, no. 1, pp. 340-347, 2003.

[32]   N. Rezlescu, E. Rezlescu, F. Tudorache *et al.*, "MgCu nanocrystalline ceramic with La3+ and Y3+ ionic substitutions used as humidity sensor," *J. Optoelectron. Adv. Mater*, vol. 6, pp. 695, 2004.

[33]   E. Melagiriyappa, and H. Jayanna, "Structural and magnetic susceptibility studies of samarium substituted magnesium–zinc ferrites," *Journal of Alloys and Compounds*, vol. 482, no. 1, pp. 147-150, 2009.

[34]   R. M. Cornell, and U. Schwertmann, *The iron oxides: structure, properties, reactions, occurrences and uses*: John Wiley & Sons, 2003.

[35]   R. Conell, and U. Schertmann, "The iron oxides: structure, properties, reactions, occurrence and uses," *Verlagsgesellschaft mbH (VHC)*, 1996.

[36]   W. Wu, Z. Wu, T. Yu *et al.*, "Recent progress on magnetic iron oxide nanoparticles: synthesis, surface functional strategies and biomedical applications," *Science and Technology of Advanced Materials*, vol. 16, no. 2, pp. 023501, 2016.

[37]   D. Zins, V. Cabuil, and R. Massart, "New aqueous magnetic fluids," *Journal of Molecular Liquids*, vol. 83, no. 1, pp. 217-232, 1999.

[38]   J. W. Bulte, "Intracellular endosomal magnetic labeling of cells," *Magnetic Resonance Imaging: Methods and Biologic Applications*, pp. 419-439, 2006.

[39]   A. K. Gupta, and M. Gupta, "Synthesis and surface engineering of iron oxide nanoparticles for biomedical applications," *Biomaterials*, vol. 26, no. 18, pp. 3995-4021, 2005.

[40]   C. Piconi, and G. Maccauro, "Zirconia as a ceramic biomaterial," *Biomaterials,* vol. 20, no. 1, pp. 1-25, 1999.

[41]   L. Malavasi, C. A. Fisher, and M. S. Islam, "Oxide-ion and proton conducting electrolyte materials for clean energy applications: structural and mechanistic features," *Chemical Society Reviews,* vol. 39, no. 11, pp. 4370-4387, 2010.

[42]   T. Vagkopoulou, "Zirconia in dentistry: part 2. Evidence-based clinical breakthrough," Department of Prosthodontics, School of Dentistry, Albert-Ludwigs University, Freiburg, Germany, 2009.

[43]   I. Denry, and J. R. Kelly, "State of the art of zirconia for dental applications," *Dental materials,* vol. 24, no. 3, pp. 299-307, 2008.

[44]   M. Rashad, and H. Baioumy, "Effect of thermal treatment on the crystal structure and morphology of zirconia nanopowders produced by three different routes," *journal of materials processing technology,* vol. 195, no. 1, pp. 178-185, 2008.

[45]   S. Laurent, D. Forge, M. Port *et al.,* "Magnetic iron oxide nanoparticles: synthesis, stabilization, vectorization, physicochemical characterizations, and biological applications," *Chemical reviews,* vol. 108, no. 6, pp. 2064-2110, 2008.

[46]   W. Wu, Q. He, and C. Jiang, "Magnetic iron oxide nanoparticles: synthesis and surface functionalization strategies," *ChemInform,* vol. 40, no. 24, pp. i, 2009.

[47]   R. H. Kodama, and A. E. Berkowitz, "Atomic-scale magnetic modeling of oxide nanoparticles," *Physical Review B,* vol. 59, no. 9, pp. 6321, 1999.

[48]   T. Sugimoto, *Fine particles: synthesis, characterization, and mechanisms of growth*: CRC Press, 2000.

[49]   C. Bean, and J. Livingston, "Superparamagnetism," *Journal of Applied Physics,* vol. 30, no. 4, pp. S120-S129, 1959.

[50]   R. Kodama, "Magnetic nanoparticles," *Journal of Magnetism and Magnetic Materials,* vol. 200, no. 1, pp. 359-372, 1999.

[51]   L. Harris, J. Goff, A. Carmichael *et al.,* "Magnetite nanoparticle dispersions stabilized with triblock copolymers," *Chemistry of Materials,* vol. 15, no. 6, pp. 1367-1377, 2003.

[52]   S. Sheng-Nan, W. Chao, Z. Zan-Zan *et al.,* "Magnetic iron oxide nanoparticles: Synthesis and surface coating techniques for biomedical applications," *Chinese Physics B,* vol. 23, no. 3, pp. 037503, 2014.

[53]   W. Wu, Q. He, and C. Jiang, "Magnetic iron oxide nanoparticles: synthesis and surface functionalization strategies," *Nanoscale Research Letters,* vol. 3, no. 11, pp. 397, 2008.

[54]   M. Chirita, I. Grozescu, L. Taubert *et al.,* "Fe2O3–nanoparticles, physical properties and their photochemical and photoelectrochemical applications," *Chem. Bull,* vol. 54, no. 68, pp. 1-8, 2009.

[55]   K. Nadeem, H. Krenn, and D. Szabó, "Influence of surface spins on the magnetization of fine maghemite nanoparticles." pp. 347-350.

[56]   M. Islam, J. Kurawaki, Y. Kusumoto *et al.,* "Hydrothermal novel synthesis of neck-structured hyperthermia-suitable magnetic (Fe_3O_4, γ-Fe_2O_3 and α-Fe_2O_3) nanoparticles," *Journal of Scientific Research,* vol. 4, no. 1, pp. 99, 2011.

[57]   K. Nadeem, H. Krenn, T. Traussnig *et al.,* "Effect of dipolar and exchange interactions on magnetic blocking of maghemite nanoparticles," *Journal of Magnetism and Magnetic Materials,* vol. 323, no. 15, pp. 1998-2004, 2011.

[58] E. A. Osborne, T. M. Atkins, D. A. Gilbert *et al.*, "Rapid microwave-assisted synthesis of dextran-coated iron oxide nanoparticles for magnetic resonance imaging," *Nanotechnology,* vol. 23, no. 21, pp. 215602, 2012.

[59] K. Nadeem, H. Krenn, T. Traussnig *et al.*, "Spin-glass freezing of maghemite nanoparticles prepared by microwave plasma synthesis," *Journal of Applied Physics,* vol. 111, no. 11, pp. 113911, 2012.

[60] Y.-H. Deng, C.-C. Wang, J.-H. Hu *et al.*, "Investigation of formation of silica-coated magnetite nanoparticles via sol–gel approach," *Colloids and Surfaces A: Physicochemical and Engineering Aspects,* vol. 262, no. 1, pp. 87-93, 2005.

[61] M. Benitez, D. Mishra, P. Szary *et al.*, "Structural and magnetic characterization of self-assembled iron oxide nanoparticle arrays," *Journal of Physics: Condensed Matter,* vol. 23, no. 12, pp. 126003, 2011.

[62] Y. Zhang, and J. Zhang, "First principles study of structural and thermodynamic properties of zirconia," *Materials Today: Proceedings,* vol. 1, no. 1, pp. 44-54, 2014.

[63] G. Cao, *Synthesis, properties and applications*: World Scientific, 2004.

[64] P. Saravanan, R. Gopalan, and V. Chandrasekaran, "Synthesis and characterisation of nanomaterials," *Defence Science Journal,* vol. 58, no. 4, pp. 504, 2008.

[65] S. Verma, R. Gokhale, and D. J. Burgess, "A comparative study of top-down and bottom-up approaches for the preparation of micro/nanosuspensions," *International journal of pharmaceutics,* vol. 380, no. 1, pp. 216-222, 2009.

[66] L. Ai, and J. Jiang, "Influence of annealing temperature on the formation, microstructure and magnetic properties of spinel nanocrystalline cobalt ferrites," *Current Applied Physics,* vol. 10, no. 1, pp. 284-288, 2010.

[67] H. Yang, X. Zhang, W. Ao *et al.*, "Formation of NiFe 2 O 4 nanoparticles by mechanochemical reaction," *Materials Research Bulletin,* vol. 39, no. 6, pp. 833-837, 2004.

[68] A. S. Teja, and P.-Y. Koh, "Synthesis, properties, and applications of magnetic iron oxide nanoparticles," *Progress in crystal growth and characterization of materials,* vol. 55, no. 1, pp. 22-45, 2009.

[69] D. Vollath, and D. V. Szabó, "The Microwave plasma process–a versatile process to synthesise nanoparticulate materials," *Journal of Nanoparticle Research,* vol. 8, no. 3-4, pp. 417-428, 2006.

[70] D. Vollath, D. Szabo, R. Taylor *et al.*, "Synthesis and magnetic properties of nanostructured maghemite," *Journal of materials research,* vol. 12, no. 08, pp. 2175-2182, 1997.

[71] D. Vollath, and K. E. Sickafus, "Synthesis of nanosized ceramic oxide powders by microwave plasma reactions," *Nanostructured Materials,* vol. 1, no. 5, pp. 427-437, 1992.

[72] D. Vollath, D. Szabo, R. Taylor *et al.*, "Synthesis and properties of nanocrystalline superparamagnetic γ-Fe 2 O 3," *Nanostructured Materials,* vol. 6, no. 5, pp. 941-944, 1995.

[73] "Phase Diagrams for Ceramists," *American Ceramic Society, 1969,* pp. p. 5.

[74] D. Vollath, and K. E. Sickafus, "Synthesis of ceramic oxide powders in a microwave plasma device," *Journal of materials research,* vol. 8, no. 11, pp. 2978-2984, 1993.

[75] L. Kazmerski, M. Ayyagari, G. Sanborn *et al.*, "Electron and X-ray diffraction analyses of ternary compound (I–III–VI2) thin films," *Thin Solid Films,* vol. 37, no. 3, pp. 323-334, 1976.

[76] V. Rajendran, *Materials Sc*: Tata McGraw-Hill Education, 2004.
[77] W. D. K. D. Brandon, *Microstructural Characterization of Materials*, 2nd edition ed.: John Wiley and Sons, 2008.
[78] B. D. Cullity, *Elements of X-Ray Diffraction*: Addison-Wesley, 1956.
[79] J. B. Pendry, "Low-energy electron diffraction," *Interaction of Atoms and Molecules with Solid Surfaces*, pp. 201-211: Springer, 1990.
[80] H. Cole, "Bragg's law and energy sensitive detectors," *Journal of Applied Crystallography*, vol. 3, no. 5, pp. 405-406, 1970.
[81] B. Tanner, T. Hase, J. Clarke *et al.*, "High resolution X-ray scattering from nanotechnology materials," *Applied surface science*, vol. 182, no. 3, pp. 202-208, 2001.
[82] J. L. Amorós, *The Laue Method*: Elsevier, 2012.
[83] S. O. Pillai, *Solid state physics*, p.^pp. 168: New age international, 2005.
[84] A. Patterson, "The Scherrer formula for X-ray particle size determination," *Physical review*, vol. 56, no. 10, pp. 978, 1939.
[85] R. Wirth, "Focused Ion Beam (FIB) combined with SEM and TEM: Advanced analytical tools for studies of chemical composition, microstructure and crystal structure in geomaterials on a nanometre scale," *Chemical Geology*, vol. 261, no. 3, pp. 217-229, 2009.
[86] D. Brandon, and W. D. Kaplan, *Microstructural characterization of materials*: John Wiley & Sons, 2013.
[87] T. Ryhänen, H. Seppä, R. Ilmoniemi *et al.*, "SQUID magnetometers for low-frequency applications," *Journal of Low Temperature Physics*, vol. 76, no. 5-6, pp. 287-386, 1989.
[88] B. D. Josephson, "Possible new effects in superconductive tunnelling," *Physics letters*, vol. 1, no. 7, pp. 251-253, 1962.
[89] P. W. J. Atkins, L. L., *Chemical principles: the quest for insight*, 3rd Edition ed. ed.: W.H. Freeman and Company, 2005.
[90] R. H. Kodama, A. E. Berkowitz, E. McNiff Jr *et al.*, "Surface spin disorder in $NiFe_2O_4$ nanoparticles," *Physical Review Letters*, vol. 77, no. 2, pp. 394, 1996.
[91] H. Blythe, V. Fedosyuk, O. Kasyutich *et al.*, "SQUID studies of Co–Cu heterogeneous alloy nanowires," *Journal of magnetism and magnetic materials*, vol. 208, no. 3, pp. 251-254, 2000.
[92] K. Vandervoort, G. Griffith, H. Claus *et al.*, "A low field SQUID magnetometer system for magnetic characterization of high-Tc superconducting samples," *Review of scientific instruments*, vol. 62, no. 9, pp. 2271-2275, 1991.
[93] T. Mathew, S. Malwadkar, S. Pai *et al.*, "Oxidative Dehydrogenation of Ethylbenzene over $Cu_{1-x}Co_xFe_2O_4$ Catalyst System: Influence of Acid–Base Property," *Catalysis letters*, vol. 91, no. 3-4, pp. 217-224, 2003.
[94] R. Hergt, R. Hiergeist, I. Hilger *et al.*, "Maghemite nanoparticles with very high AC-losses for application in RF-magnetic hyperthermia," *Journal of Magnetism and Magnetic Materials*, vol. 270, no. 3, pp. 345-357, 2004.
[95] X. Xu, Y. Wolfus, A. Shaulov *et al.*, "Annealing study of Fe_2O_3 nanoparticles: Magnetic size effects and phase transformations," *Journal of applied physics*, vol. 91, pp. 4611-4616, 2002.
[96] D. Maiti, U. Manju, S. Velaga *et al.*, "Phase evolution and growth of iron oxide nanoparticles: Effect of hydrazine addition during sonication," *Crystal Growth & Design*, vol. 13, no. 8, pp. 3637-3644, 2013.

[97] Y. Uhm, W. Kim, and C. Rhee, "A study of synthesis and phase transition of nanofibrous Fe 2 O 3 derived from hydrolysis of Fe nanopowders," *Scripta materialia,* vol. 50, no. 5, pp. 561-564, 2004.

[98] K. Nadeem, L. Ali, I. Gul *et al.,* "Effect of silica coating on the structural, dielectric, and magnetic properties of maghemite nanoparticles," *Journal of Non-Crystalline Solids,* vol. 404, pp. 72-77, 2014.

[99] R. Grau-Crespo, A. Y. Al-Baitai, I. Saadoune *et al.,* "Vacancy ordering and electronic structure of γ-Fe2O3 (maghemite): a theoretical investigation," *Journal of Physics: Condensed Matter,* vol. 22, no. 25, pp. 255401, 2010.

[100] C. Corot, P. Robert, J.-M. Idée *et al.,* "Recent advances in iron oxide nanocrystal technology for medical imaging," *Advanced drug delivery reviews,* vol. 58, no. 14, pp. 1471-1504, 2006.

[101] R. Bosisio, M. Wertheimer, and C. Weissfloch, "Generation of large volume microwave plasmas," *Journal of Physics E: Scientific Instruments,* vol. 6, no. 7, pp. 628, 1973.

[102] J. Jiang, Y.-M. Yang, and L.-C. Li, "Effect of heat treatment on the magnetic properties of nanocrystalline spinel Li–Ni ferrite prepared by a simple soft chemistry route," *Journal of Alloys and Compounds,* vol. 464, no. 1, pp. 370-373, 2008.

[103] K. H. Wu, Y. C. Chang, and G. P. Wang, "Preparation of NiZn ferrite/SiO 2 nanocomposite powders by sol–gel auto-combustion method," *Journal of magnetism and magnetic materials,* vol. 269, no. 2, pp. 150-155, 2004.

[104] K. Thummer, M. Chhantbar, K. Modi *et al.,* "Localized canted spin behaviour in ZnxMg1. 5– xMn0. 5FeO4spinelferritesystem," *Journal of magnetism and magnetic materials,* vol. 280, no. 1, pp. 23-30, 2004.

[105] L. Machala, R. Zboril, and A. Gedanken, "Amorphous iron (III) oxide a review," *The Journal of Physical Chemistry B,* vol. 111, no. 16, pp. 4003-4018, 2007.

[106] R. Zboril, L. Machala, M. Mashlan *et al.,* "Magnetism of amorphous Fe2O3 nanopowders synthesized by solid-state reactions," *physica status solidi (c),* vol. 1, no. 12, pp. 3710-3716, 2004.

[107] Z. Zi, Y. Sun, X. Zhu *et al.,* "Synthesis and magnetic properties of CoFe 2 O 4 ferrite nanoparticles," *Journal of Magnetism and Magnetic Materials,* vol. 321, no. 9, pp. 1251-1255, 2009.

[108] E. V. Gopalan, P. Joy, I. Al-Omari *et al.,* "On the structural, magnetic and electrical properties of sol–gel derived nanosized cobalt ferrite," *Journal of Alloys and Compounds,* vol. 485, no. 1, pp. 711-717, 2009.

[109] J. William D. Callister, *material science and Engineering: An Introduction*: John Wiley&Sons, 2000.

[110] E. TRONC, "Magnetic relaxation in fine-particle systems," *Advances in,* pp. 283, 1997.

[111] X. Batlle, and A. Labarta, "Finite-size effects in fine particles: magnetic and transport properties," *Journal of Physics D: Applied Physics,* vol. 35, no. 6, pp. R15, 2002.

[112] M. Benitez, P. Szary, D. Mishra *et al.,* "Templated self-assembly of iron oxide nanoparticles," *arXiv preprint arXiv:1010.4166,* 2010.

[113] A. R. Mary, T. Narayanan, V. Sunny *et al.,* "Synthesis of Bio-Compatible SPION–based Aqueous Ferrofluids and Evaluation of RadioFrequency Power Loss for Magnetic Hyperthermia," *Nanoscale research letters,* vol. 5, no. 10, pp. 1706, 2010.

[114] X. Lin, C. Sorensen, K. Klabunde *et al.*, "Temperature dependence of morphology and magnetic properties of cobalt nanoparticles prepared by an inverse micelle technique," *Langmuir,* vol. 14, no. 25, pp. 7140-7146, 1998.

[115] B. Martinez, X. Obradors, L. Balcells *et al.*, "Low temperature surface spin-glass transition in γ-Fe 2 O 3 nanoparticles," *Physical Review Letters,* vol. 80, no. 1, pp. 181, 1998.

[116] J. Smit, and H. P. J. Wijn, *Ferrites: physical properties of ferrimagnetic oxides in relation to their technical applications*: Wiley, 1959.

[117] C. Verdes, B. Ruiz-Diaz, S. Thompson *et al.*, "Computational model of the magnetic and transport properties of interacting fine particles," *Physical Review B,* vol. 65, no. 17, pp. 174417, 2002.

[118] F. Bloch, "Zur theorie des ferromagnetismus," *Zeitschrift für Physik,* vol. 61, no. 3-4, pp. 206-219, 1930.

[119] H. Zijlstra, and E. Wohlfarth, "Ferromagnetic Materials, vol. 3North-Holland," Amsterdam, 1982.

[120] K. Maaz, A. Mumtaz, S. Hasanain *et al.*, "Temperature dependent coercivity and magnetization of nickel ferrite nanoparticles," *Journal of Magnetism and Magnetic Materials,* vol. 322, no. 15, pp. 2199-2202, 2010.

[121] S. Singhal, J. Singh, S. Barthwal *et al.*, "Preparation and characterization of nanosize nickel-substituted cobalt ferrites (Co 1− xNixFe 2 O 4)," *Journal of Solid State Chemistry,* vol. 178, no. 10, pp. 3183-3189, 2005.

[122] J. B. Goodenough, "A theory of domain creation and coercive force in polycrystalline ferromagnetics," *Physical Review,* vol. 95, no. 4, pp. 917, 1954.

[123] D. L. Graf, D. E. Anderson, and J. B. Woodhouse, "Ionic diffusion in naturally-occurring aqueous solutions: transition-state models that use either empirical expressions or statistically-derived relationships to predict mutual diffusion coefficients in the concentrated-solution regions of 8 binary systems," *Geochimica et Cosmochimica Acta,* vol. 47, no. 11, pp. 1985-1998, 1983.

[124] S. Bedanta, and W. Kleemann, "Supermagnetism," *Journal of Physics D: Applied Physics,* vol. 42, no. 1, pp. 013001, 2008.

[125] J. Gonzdez, M. Montero, X. Batlle *et al.*, "agnetization Reversal Mechanisms in Colloidal Dispersions of Magnetite Particles," *IEEE transactions on magnetics,* vol. 34, no. 4, 1998.

[126] S. Shtrikman, and E. Wohlfarth, "The theory of the Vogel-Fulcher law of spin glasses," *Physics Letters A,* vol. 85, no. 8-9, pp. 467-470, 1981.

[127] K. Fischer, and J. Hertz, "Spin-Glasses, volume 1 of Cambridge Studies in Magnetism," Cambridge university press, Cambridge, 1991.

[128] D. Fiorani, A. Testa, F. Lucari *et al.*, "Magnetic properties of maghemite nanoparticle systems: surface anisotropy and interparticle interaction effects," *Physica B: Condensed Matter,* vol. 320, no. 1, pp. 122-126, 2002.

[129] G. C. Papaefthymiou, "Nanoparticle magnetism," *Nano Today,* vol. 4, no. 5, pp. 438-447, 2009.